Overall response of viscoelastic composites and polycrystals: exact asymptotic relations and approximate estimates

Renald Brenner, Pierre Suquet

Overall response of viscoelastic composites and polycrystals: exact asymptotic relations and approximate estimates

R. Brenner[a], P. Suquet[b]

[a]*Institut Jean Le Rond d'Alembert, Université Pierre et Marie Curie, CNRS, UMR 7190, 4 place Jussieu, 75252 Paris Cedex 05, France*
[b]*Laboratoire de Mécanique et d'Acoustique, CNRS, UPR 7051 31 chemin Joseph Aiguier. 13402 Marseille Cedex 20, France*

Abstract

This paper is devoted to the effective behavior of linear viscoelastic heterogeneous materials with a particular emphasis on their transient response. First, two new asymptotic relations for the overall creep function are derived at short and large times. They are related to the retardation spectrum of the composite and involve second-order moments per phase of the stress field for the purely elastic and purely viscous problems. In the context of harmonic loadings, these relations provide exact frequential asymptotic conditions on the overall storage and loss moduli. Second, by making use of these asymptotic results, an approximate model is proposed. It consists in approximating the retardation spectrum of the composite by a single discrete Dirac mass. Its accuracy is assessed by comparison with exact analytical results, full-field simulations and collocation results for several classes of composites and polycrystals.

Keywords: linear viscoelasticity, homogenization, effective creep function, particulate composites, polycrystals

Email addresses: renald.brenner@upmc.fr (R. Brenner), suquet@lma.cnrs-mrs.fr (P. Suquet)

1. Introduction

A major issue in the determination of the effective properties of viscoelastic composites or polycrystals is the description of the interaction between elastic and viscous deformation mechanisms within the material. The present study is a contribution towards the understanding of this coupling.

The local and overall constitutive relations between the infinitesimal strain $\boldsymbol{\varepsilon}$ and the Cauchy stress $\boldsymbol{\sigma}$ fields can be expressed as hereditary integrals. At the scale of individual constituents it reads

$$\boldsymbol{\varepsilon}(\boldsymbol{x},t) = \left(\boldsymbol{M}^{(r)} \star \boldsymbol{\sigma}\right)(\boldsymbol{x},t), \tag{1}$$

where $\boldsymbol{x}$ denotes a material point within phase r of the composite and $\star$ stands for the Stieljes convolution product (Appendix A). Similarly the macroscopic or *effective* constitutive relations can be written as

$$\overline{\boldsymbol{\varepsilon}}(t) = (\widetilde{\boldsymbol{M}} \star \overline{\boldsymbol{\sigma}})(t) \tag{2}$$

where $\overline{\boldsymbol{\varepsilon}}$ and $\overline{\boldsymbol{\sigma}}$ are the macroscopic, or averaged, strain and stress (the overall bar denotes spatial averaging over a representative volume element of the material). $\boldsymbol{M}^{(r)}(t)$ and $\widetilde{\boldsymbol{M}}(t)$ are the local (in phase r) and effective creep functions of the composite.

Even when the constituents have a "short memory" (for instance Kelvin-Voigt or Maxwell materials whose creep functions $\boldsymbol{M}(t)$ are characterized by a single retardation time), it is well established that the effective kernel function $\widetilde{\boldsymbol{M}}$ exhibits an additional fading memory term (*i.e.* a "long memory" effect) (Sanchez-Hubert and Sanchez-Palencia, 1978; Francfort et al., 1983; Suquet, 1987), and in particular is *not* characterized by a single retardation time. More specifically, when the individual constituents of the composite are Maxwellian, their creep function takes the form

$$\boldsymbol{M}^{(r)}(t) = \boldsymbol{M}_e^{(r)} + t\,\boldsymbol{M}_v^{(r)}, \tag{3}$$

whereas the overall creep function of the composite can be written as:

$$\widetilde{\boldsymbol{M}}(t) = \widetilde{\boldsymbol{M}}_0 + t\,\widetilde{\boldsymbol{M}}_\infty + \int_0^{+\infty} \widetilde{\boldsymbol{J}}(\tau)\,(1 - \mathrm{e}^{-t/\tau})\,\mathrm{d}\tau \tag{4}$$

where $\widetilde{\boldsymbol{M}}_0 + t\,\widetilde{\boldsymbol{M}}_\infty$ is the Maxwellian component of $\widetilde{\boldsymbol{M}}(t)$ (corresponding to "short memory" effects as in (3)) and $\widetilde{\boldsymbol{J}}(\tau)$ is the retardation spectrum

associated with "long memory" effects. The different terms $\widetilde{\boldsymbol{M}}_0$, $\widetilde{\boldsymbol{M}}_\infty$ and $\widetilde{\boldsymbol{J}}$ can be interpreted in physical terms by analyzing the response of the composite to a creep test (see Subsection 2.2 and Figure 1). For simplicity the present study will be focused on Maxwellian individual constituents, corresponding for instance to irradiation creep in metals or ceramics at high temperature. However it is worth noting that the long-memory effects have a general character and that some of the conclusions of our study apply to more general viscoelastic behaviors of the constituents.

These long-memory effects, arising from the change of scales, can be evidenced by means of the correspondence principle (Mandel, 1966) by which the original viscoelastic problem is transformed into a symbolic elastic one (Hashin, 1965, 1970; Laws and Mc Laughlin, 1978; Turner and Tomé, 1993). The effective kernel $\widetilde{\boldsymbol{J}}(\tau)$ can then be tabulated at the expense of computing a large number of effective moduli to obtain the Laplace transform $\widetilde{\boldsymbol{M}}^*(p)$ of $\widetilde{\boldsymbol{M}}(t)$ for a large number of Laplace parameters p and then by taking the inverse Laplace transform of $\widetilde{\boldsymbol{M}}^*(p)$. In a few specific cases, $\widetilde{\boldsymbol{J}}(\tau)$ can even be derived in closed form (Rougier et al., 1993; Masson et al., 2012). However, even when $\widetilde{\boldsymbol{J}}$ is known, either in tabulated form or in closed form, the implementation of constitutive laws with long-memory effects in a macroscopic structural computation requires to store the whole time history of the overall stress (or strain) at each Gauss point of the structure. The computational cost of this storage is prohibitive and approximate methods to avoid it have been developed, proceeding either by a direct step-by-step integration in time of the effective constitutive relations (Lahellec and Suquet, 2007; Kowalczyk-Gajewska and Petryk, 2011), or by approximating the relaxation kernel of the composite. In the latter approach, a common practice, which goes back to Schapery (1974) and Laws and Mc Laughlin (1978), consists in approximating the effective kernel function by a finite sum of decaying exponentials (so-called Prony series). This approximation turns out to be exact only if the relaxation (or equivalently retardation) spectrum consists of discrete Dirac masses corresponding to a finite number of relaxation times. This is the case, for instance, when the microstructure of the composite is such that the Hashin-Shtrikman's estimate for isotropic two-phase composites is appropriate to estimate the effective linear (either purely elastic or purely viscous) properties of the composite (Brenner and Masson, 2005; Ricaud and Masson, 2009). It is also the case for the bulk relaxation of isotropic composites composed of the assemblage of coated inclusions (Beurthey and Zaoui,

2000) for which the generalized self-consistent estimate (a.k.a. $N+1$ – phase model) applies. In more general situations, the exact effective spectrum has a continuous part and the Prony series provide only a convenient approximation. The widely used collocation method and its extensions rely on this series approximation (Schapery, 1962; Cost and Becker, 1970; Bradshaw and Brinson, 1997; Turner and Tomé, 1993; Masson and Zaoui, 1999; Rekik and Brenner, 2011).

New results have recently been obtained on the effective relaxation function of linear viscoelastic composites by considering its asymptotic behavior in time (Suquet, 2012). These exact relations, which imply restrictions on the effective relaxation function, involve cross products of elastic stress fields with viscous compliances (viscous dissipation due to elastic or short-term stress fields) and cross products of viscous stress fields with elastic compliances (elastic energy stored in long-term stress fields). Moreover, by making use of the Prony series approximation, they can be used to construct a model with only two relaxation times for incompressible materials with overall isotropy. This model is exact for specific microstructures whose relaxation spectrum consists precisely of two discrete Dirac masses.

Following these results, the motivation of the present work is threefold. First, we aim at deriving corresponding asymptotic relations for the overall *creep* function. To this aim, the instantaneous and delayed local and global responses of the composite to a creep test are analyzed. Second, the physical interpretation of these conditions on the overall response is given for various mechanical loadings. These relations have implications on the retardation $\widetilde{\boldsymbol{J}}(\tau)$ and relaxation $\widetilde{\boldsymbol{G}}(\tau)$ spectra and on the storage $\widetilde{\boldsymbol{L}}'(\omega)$ and loss $\widetilde{\boldsymbol{L}}''(\omega)$ moduli characterizing the harmonic steady-state response of the composite at frequency ω. Third, we derive the dual formulation of the approximate model of Suquet (2012). It is then applied to estimate the overall viscoelastic response of isotropic composites with particulate or granular microstructures. Its accuracy is assessed by comparisons with analytical results, with the standard collocation method as well as with full-field computations performed with the fast Fourier transform (FFT) method (Moulinec and Suquet, 1998; Labé et al., 2011).

2. Composites with Maxwellian constituents

2.1. Local problem

The composite materials considered in this study are made from N different homogeneous constituents, or phases, which are assumed to be randomly distributed in a representative volume element V and perfectly bonded across their interfaces. Each constituent occupies a domain V_r with characteristic function $\chi^{(r)}$. The total and partial volume averages of a function f over the entire volume V and over phase r are denoted by $\overline{f}$ and $\overline{f}^{(r)}$ respectively. The phases are linearly viscoelastic and Maxwellian, characterized by elastic and viscous compliances $\boldsymbol{M}_e^{(r)}$ and $\boldsymbol{M}_v^{(r)}$ (with inverse $\boldsymbol{L}_e^{(r)}$ and $\boldsymbol{L}_v^{(r)}$) and governed by the constitutive relations

$$\dot{\boldsymbol{\varepsilon}}(\boldsymbol{x},t) = \boldsymbol{M}_e^{(r)} : \dot{\boldsymbol{\sigma}}(\boldsymbol{x},t) + \boldsymbol{M}_v^{(r)} : \boldsymbol{\sigma}(\boldsymbol{x},t) \text{ in phase } r. \tag{5}$$

The initial conditions are taken such that the material is initially at rest:

$$\boldsymbol{\varepsilon}(\boldsymbol{x},t) = \boldsymbol{\sigma}(\boldsymbol{x},t) = \boldsymbol{0} \quad \text{for all } t < 0. \tag{6}$$

Defining

$$\boldsymbol{M}_e(\boldsymbol{x}) = \sum_{r=1}^{N} \boldsymbol{M}_e^{(r)} \chi^{(r)}(\boldsymbol{x}), \quad \boldsymbol{M}_v(\boldsymbol{x}) = \sum_{r=1}^{N} \boldsymbol{M}_v^{(r)} \chi^{(r)}(\boldsymbol{x}),$$

the local stress and strain fields $\boldsymbol{\sigma}(\boldsymbol{x},t)$ and $\boldsymbol{\varepsilon}(\boldsymbol{x},t)$ are determined by resolution of the so-called *local problem* consisting of the constitutive relations of the phases, the equilibrium and compatibility equations, and a prescribed history of overall stress or strain:

$$\left.\begin{array}{l} \dot{\boldsymbol{\varepsilon}}(\boldsymbol{x},t) = \boldsymbol{M}_e(\boldsymbol{x}) : \dot{\boldsymbol{\sigma}}(\boldsymbol{x},t) + \boldsymbol{M}_v(\boldsymbol{x}) : \boldsymbol{\sigma}(\boldsymbol{x},t), \quad \text{for } (\boldsymbol{x},t) \in V \times [0,T], \\ \text{div } \boldsymbol{\sigma} = \boldsymbol{0}, \quad \boldsymbol{\varepsilon}(\boldsymbol{x},t) = \frac{1}{2}\left(\boldsymbol{\nabla}\boldsymbol{u} + \boldsymbol{\nabla}\boldsymbol{u}^{\mathrm{T}}\right)(\boldsymbol{x},t), \qquad \text{for } (\boldsymbol{x},t) \in V \times [0,T], \\ \langle \boldsymbol{\sigma}(t) \rangle = \overline{\boldsymbol{\sigma}}(t) + \text{ boundary conditions on } \partial V. \end{array}\right\} \tag{7}$$

The boundary conditions on ∂V can be either periodicity conditions, uniform traction, affine displacement or others, provided that Hill's lemma applies (see Ponte Castañeda and Suquet, 1998, for details). The size of the volume element V is assumed to be sufficiently large, compared to the size of the heterogeneities, to ensure that the boundary conditions do not affect significantly the effective response of the composite.

The effective or homogenized constitutive relations link the average strain $\overline{\boldsymbol{\varepsilon}}(t)$ at time t to the history of average stress prior to t, $\overline{\boldsymbol{\sigma}}(s), 0 \leq s \leq t$ and take the integral form (2). The material function characterizing the viscoelastic properties of the composite is the effective creep kernel $\widetilde{\boldsymbol{M}}(t)$ which can be obtained by analyzing the overall strain response of the volume element V to a creep test.

2.2. Response of the composite to a creep test

The applied overall stress in a creep test reads as

$$\overline{\boldsymbol{\sigma}}(t) = \mathbf{0} \quad \text{for all} \quad t < 0, \quad \overline{\boldsymbol{\sigma}}(t) = \overline{\boldsymbol{\sigma}} \quad \text{for all} \quad t \geq 0. \tag{8}$$

The overall stress is a discontinuous function of time at $t = 0$ and its time derivative is therefore a Dirac mass at $t = 0$. The Stieljes integral has to be interpreted in a generalized sense as detailed in Appendix A. From relations (2) and (A.2), it is found that the overall strain response of the composite is directly related to the effective kernel $\widetilde{\boldsymbol{M}}(t)$, through:

$$\overline{\boldsymbol{\varepsilon}}(t) = \widetilde{\boldsymbol{M}}(t) : \overline{\boldsymbol{\sigma}} = \left(\widetilde{\boldsymbol{M}}_0 + t\, \widetilde{\boldsymbol{M}}_\infty + \int_0^{+\infty} \widetilde{\boldsymbol{J}}(\tau)\, (1 - \mathrm{e}^{-t/\tau})\, \mathrm{d}\tau \right) : \overline{\boldsymbol{\sigma}}, \tag{9}$$

and the overall strain rate is:

$$\dot{\overline{\boldsymbol{\varepsilon}}}(t) = \left(\widetilde{\boldsymbol{M}}_\infty + \int_0^{+\infty} \frac{\widetilde{\boldsymbol{J}}(\tau)}{\tau}\, \mathrm{e}^{-t/\tau}\, \mathrm{d}\tau \right) : \overline{\boldsymbol{\sigma}}. \tag{10}$$

The different terms in these expressions can be interpreted as follows (see Figure 1):

1. $\widetilde{\boldsymbol{M}}_0$ characterizes the instantaneous response of the composite:
$$\overline{\boldsymbol{\varepsilon}}(0^+) = \widetilde{\boldsymbol{M}}_0 : \overline{\boldsymbol{\sigma}}.$$
2. $\widetilde{\boldsymbol{M}}_\infty$ characterizes the long-term (or delayed) response of the composite:
$$\dot{\overline{\boldsymbol{\varepsilon}}}(+\infty) = \widetilde{\boldsymbol{M}}_\infty : \overline{\boldsymbol{\sigma}}.$$
3. The "Maxwellian" component of $\widetilde{\boldsymbol{M}}(t)$ (short-memory effects) is defined as:
$$\widetilde{\boldsymbol{M}}^{Maxw}(t) = \widetilde{\boldsymbol{M}}_0 + t\widetilde{\boldsymbol{M}}_\infty. \tag{11}$$

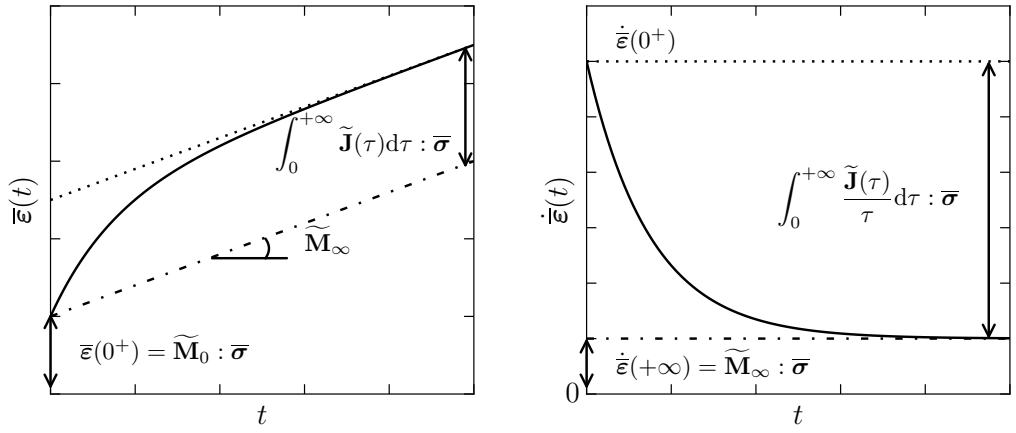

Figure 1: Interpretation of the short and long memory terms in the effective creep kernel. Overall creep strain (left) and overall creep strain-rate (right) for a constant applied macroscopic stress $\overline{\boldsymbol{\sigma}}$. Exact response (solid line) and Maxwell approximation (dot-dashed line)

It is shown as a dot-dashed line in Figure 1. The long-memory effects of the effective constitutive relations are contained in the kernel $\widetilde{\boldsymbol{J}}$. Taking the limit of (9) as $t \to +\infty$, it is seen that the integral $\displaystyle\int_0^{+\infty} \widetilde{\boldsymbol{J}}(\tau)\,\mathrm{d}\tau : \overline{\boldsymbol{\sigma}}$ is the *additional creep strain* due to long memory effects, which adds up to the creep strain due to the Maxwellian component of $\widetilde{\boldsymbol{M}}(t)$.

4. Taking the limit of (10) as $t \to 0^+$, it is found that $\displaystyle\int_0^{+\infty} \frac{\widetilde{\boldsymbol{J}}(\tau)}{\tau}\,\mathrm{d}\tau : \overline{\boldsymbol{\sigma}}$ is the difference between the instantaneous strain-rate (at $t = 0^+$) and the delayed strain-rate $\widetilde{\boldsymbol{M}}_\infty : \overline{\boldsymbol{\sigma}}$ as $t \to +\infty$.

2.3. Local response of the composite to a creep test at short and large time

The solution $(\boldsymbol{\sigma}(\boldsymbol{x},t), \boldsymbol{\varepsilon}(\boldsymbol{x},t))$ of the local problem (7) has the following asymptotic properties when the volume element is subjected to a creep test.

Instantaneous response. The instantaneous response of the composite to a creep test corresponds to the limit of $(\boldsymbol{\sigma}(\boldsymbol{x},t), \boldsymbol{\varepsilon}(\boldsymbol{x},t))$ as $t \to 0^+$ (the limit is taken from the right, for $t > 0$) and depends only on the elastic properties of the phases:

$$\lim_{t\to 0^+} \boldsymbol{\sigma}(\boldsymbol{x},t) = \boldsymbol{\sigma}_e(\boldsymbol{x}), \quad \lim_{t\to 0^+} \boldsymbol{\varepsilon}(\boldsymbol{x},t) = \boldsymbol{\varepsilon}_e(\boldsymbol{x}), \tag{12}$$

where $(\boldsymbol{\sigma}_e, \boldsymbol{\varepsilon}_e)$ is the solution of the purely elastic problem

$$\boldsymbol{\varepsilon}_e(\boldsymbol{x}) = \frac{1}{2}\left(\boldsymbol{\nabla}\boldsymbol{u}_e + \boldsymbol{\nabla}\boldsymbol{u}_e^{\mathrm{T}}\right) = \boldsymbol{M}_e(\boldsymbol{x}) : \boldsymbol{\sigma}_e(\boldsymbol{x}),\ \mathrm{div}\ \boldsymbol{\sigma}_e = \boldsymbol{0},\ \langle \boldsymbol{\sigma}_e \rangle = \overline{\boldsymbol{\sigma}}. \quad (13)$$

Delayed response. The delayed response of the composite to a creep test corresponds to the limit as $t \to +\infty$ and depends only on the viscous properties of the phases:

$$\lim_{t\to+\infty} \boldsymbol{\sigma}(\boldsymbol{x}, t) = \boldsymbol{\sigma}_v(\boldsymbol{x}), \quad \lim_{t\to+\infty} \dot{\boldsymbol{\varepsilon}}(\boldsymbol{x}, t) = \dot{\boldsymbol{\varepsilon}}_v(\boldsymbol{x}), \quad (14)$$

where $(\boldsymbol{\sigma}_v, \dot{\boldsymbol{\varepsilon}}_v)$ is the solution of the purely viscous problem

$$\dot{\boldsymbol{\varepsilon}}_v(\boldsymbol{x}) = \frac{1}{2}\left(\boldsymbol{\nabla}\dot{\boldsymbol{u}}_v + \boldsymbol{\nabla}\dot{\boldsymbol{u}}_v^{\mathrm{T}}\right) = \boldsymbol{M}_v(\boldsymbol{x}) : \boldsymbol{\sigma}_v(\boldsymbol{x}),\ \mathrm{div}\ \boldsymbol{\sigma}_v = \boldsymbol{0},\ \langle \boldsymbol{\sigma}_v \rangle = \overline{\boldsymbol{\sigma}}. \quad (15)$$

2.4. Overall response of the composite to a creep test at short and large time

Taking the volume average of the strain field in (13) and of the strain-rate field in (15), two relations are obtained for the instantaneous and delayed response of the composite to a creep test:

$$\lim_{t\to0^+} \overline{\boldsymbol{\varepsilon}}(t) = \overline{\boldsymbol{\varepsilon}}_e = \langle \boldsymbol{\varepsilon}_e \rangle = \widetilde{\boldsymbol{M}}_e : \overline{\boldsymbol{\sigma}}, \quad (16)$$

$$\lim_{t\to+\infty} \dot{\overline{\boldsymbol{\varepsilon}}}(t) = \dot{\overline{\boldsymbol{\varepsilon}}}_v = \langle \dot{\boldsymbol{\varepsilon}}_v \rangle = \widetilde{\boldsymbol{M}}_v : \overline{\boldsymbol{\sigma}}. \quad (17)$$

Two first classical relations can be obtained from these asymptotic results

$$\widetilde{\boldsymbol{M}}_0 = \lim_{t\to0^+} \widetilde{\boldsymbol{M}}(t) = \widetilde{\boldsymbol{M}}_e, \quad (18)$$

and

$$\widetilde{\boldsymbol{M}}_\infty = \lim_{t\to+\infty} \dot{\widetilde{\boldsymbol{M}}}(t) = \widetilde{\boldsymbol{M}}_v. \quad (19)$$

In other words, the instantaneous and delayed response of the composite are governed by the effective compliances, respectively purely elastic $\widetilde{\boldsymbol{M}}_e$ and purely viscous $\widetilde{\boldsymbol{M}}_v$, obtained by homogenizing the local problems (13) and (15). In addition to the two well-known relations (18) and (19), two new asymptotic relations can be established (the derivation is given in Appendix B):

$$\lim_{t\to0^+} \dot{\overline{\boldsymbol{\varepsilon}}}(t) : \overline{\boldsymbol{\sigma}} = \langle \boldsymbol{\sigma}_e : \boldsymbol{M}_v : \boldsymbol{\sigma}_e \rangle\,, \quad (20)$$

and

$$\lim_{t\to+\infty}\left(\overline{\boldsymbol{\varepsilon}}(t)-\overline{\boldsymbol{\varepsilon}}^{Maxw}(t)\right):\overline{\boldsymbol{\sigma}}=\langle\boldsymbol{\sigma}_v:\boldsymbol{M}_e:\boldsymbol{\sigma}_v\rangle-\langle\boldsymbol{\sigma}_e:\boldsymbol{M}_e:\boldsymbol{\sigma}_e\rangle\,, \tag{21}$$

with :

$$\overline{\boldsymbol{\varepsilon}}^{Maxw}(t)=\widetilde{\boldsymbol{M}}^{Maxw}(t):\overline{\boldsymbol{\sigma}}, \tag{22}$$

$\widetilde{\boldsymbol{M}}^{Maxw}$ being defined in (11). Interestingly the new relations (20) and (21) involve, in their right-hand side, the second moments of the stress fields solution of the two linear (purely elastic and purely viscous) problems (13) and (15). These second moments can be expressed as

$$\langle\boldsymbol{\sigma}_e:\boldsymbol{M}_v:\boldsymbol{\sigma}_e\rangle=\sum_{r=1}^{N}c^{(r)}\boldsymbol{M}_v^{(r)}::\langle\boldsymbol{\sigma}_e\otimes\boldsymbol{\sigma}_e\rangle^{(r)}\,,$$

where the second moment per phase of the stress field $\boldsymbol{\sigma}_e$ reads as (Bobeth and Diener, 1987; Kreher, 1990; Suquet, 1995; Ponte Castañeda and Suquet, 1998)

$$\langle\boldsymbol{\sigma}_e\otimes\boldsymbol{\sigma}_e\rangle^{(r)}=\frac{1}{c^{(r)}}\overline{\boldsymbol{\sigma}}:\frac{\partial\widetilde{\boldsymbol{M}}_e}{\partial\boldsymbol{M}_e^{(r)}}:\overline{\boldsymbol{\sigma}}.$$

Therefore

$$\langle\boldsymbol{\sigma}_e:\boldsymbol{M}_v:\boldsymbol{\sigma}_e\rangle=\sum_{r=1}^{N}\boldsymbol{M}_v^{(r)}::\left(\overline{\boldsymbol{\sigma}}:\frac{\partial\widetilde{\boldsymbol{M}}_e}{\partial\boldsymbol{M}_e^{(r)}}:\overline{\boldsymbol{\sigma}}\right). \tag{23}$$

Similarly,

$$\langle\boldsymbol{\sigma}_v:\boldsymbol{M}_e:\boldsymbol{\sigma}_v\rangle=\sum_{r=1}^{N}\boldsymbol{M}_e^{(r)}::\left(\overline{\boldsymbol{\sigma}}:\frac{\partial\widetilde{\boldsymbol{M}}_v}{\partial\boldsymbol{M}_v^{(r)}}:\overline{\boldsymbol{\sigma}}\right). \tag{24}$$

It is worth noting that the new relations (20) and (21) come at no additional cost once the elastic and viscous compliances $\widetilde{\boldsymbol{M}}_e$ and $\widetilde{\boldsymbol{M}}_v$ of the composite have been determined.

Remarks: 1. Using Hill's lemma, the two relations (20) and (21) can be alternatively expressed as:

$$\lim_{t\to0^+}\overline{\boldsymbol{\sigma}}:\left(\dot{\widetilde{\boldsymbol{M}}}(t)-\dot{\widetilde{\boldsymbol{M}}}^{Maxw}(t)\right):\overline{\boldsymbol{\sigma}}=\langle(\boldsymbol{\sigma}_e-\boldsymbol{\sigma}_v):\boldsymbol{M}_v:(\boldsymbol{\sigma}_e-\boldsymbol{\sigma}_v)\rangle\,, \tag{25}$$

$$\lim_{t\to+\infty} \overline{\boldsymbol{\sigma}} : \left(\widetilde{\boldsymbol{M}}(t) - \widetilde{\boldsymbol{M}}^{Maxw}(t)\right) : \overline{\boldsymbol{\sigma}} = \langle (\boldsymbol{\sigma}_e - \boldsymbol{\sigma}_v) : \boldsymbol{M}_e : (\boldsymbol{\sigma}_e - \boldsymbol{\sigma}_v) \rangle \,. \quad (26)$$

These relations show that the effective response of the composite to a creep test is always softer than its Maxwellian approximation.

2. The relations (20) and (21) have the following implications for the effective retardation spectrum $\widetilde{\boldsymbol{J}}$:

$$\overline{\boldsymbol{\sigma}} : \int_0^{+\infty} \frac{\widetilde{\boldsymbol{J}}(\tau)}{\tau} \,\mathrm{d}\tau : \overline{\boldsymbol{\sigma}} = \langle \boldsymbol{\sigma}_e : \boldsymbol{M}_v : \boldsymbol{\sigma}_e \rangle - \langle \boldsymbol{\sigma}_v : \boldsymbol{M}_v : \boldsymbol{\sigma}_v \rangle \,. \quad (27)$$

and

$$\overline{\boldsymbol{\sigma}} : \int_0^{+\infty} \widetilde{\boldsymbol{J}}(\tau) \,\mathrm{d}\tau : \overline{\boldsymbol{\sigma}} = \langle \boldsymbol{\sigma}_v : \boldsymbol{M}_e : \boldsymbol{\sigma}_v \rangle - \langle \boldsymbol{\sigma}_e : \boldsymbol{M}_e : \boldsymbol{\sigma}_e \rangle \,, \quad (28)$$

Therefore the two gaps between the actual response of the composite and its Maxwellian approximation, indicated by arrows in the two plots of Figure 1, are directly related to cross-products of the elastic and viscous stress fields with the viscous and elastic compliances of the phases. These relations can be further simplified by noting that:

$$\langle \boldsymbol{\sigma}_e : \boldsymbol{M}_e : \boldsymbol{\sigma}_e \rangle = \overline{\boldsymbol{\sigma}} : \widetilde{\boldsymbol{M}}_e : \overline{\boldsymbol{\sigma}}, \quad \langle \boldsymbol{\sigma}_v : \boldsymbol{M}_v : \boldsymbol{\sigma}_v \rangle = \overline{\boldsymbol{\sigma}} : \widetilde{\boldsymbol{M}}_v : \overline{\boldsymbol{\sigma}}.$$

2.5. Relaxation spectrum

For completeness, asymptotic relations for the effective relaxation function $\widetilde{\boldsymbol{L}}(t)$ in the time domain are also derived here. Note that alternative expressions have been previously obtained in Laplace space (Suquet, 2012). Consider the effective relaxation function $\widetilde{\boldsymbol{L}}(t)$ of the composite, inverse of $\widetilde{\boldsymbol{M}}(t)$ in the sense of the Stieljes convolution product, by means of which the effective constitutive relation (2) can be written as

$$\overline{\boldsymbol{\sigma}}(t) = (\widetilde{\boldsymbol{L}} \star \overline{\boldsymbol{\varepsilon}})(t), \quad (29)$$

where $\widetilde{\boldsymbol{L}}(t)$ is expressed as

$$\widetilde{\boldsymbol{L}}(t) = \int_0^{+\infty} \widetilde{\boldsymbol{G}}(\tau)\, \mathrm{e}^{-t/\tau} \,\mathrm{d}\tau. \quad (30)$$

$\widetilde{\boldsymbol{G}}(\tau)$ is the effective relaxation spectrum of the composite. The relations (18), (19), (27) and (28) have counterparts for the effective relaxation function $\widetilde{\boldsymbol{L}}$

and the effective relaxation spectrum $\widetilde{\boldsymbol{G}}$. Subject the volume element V to a test where the strain history $\overline{\boldsymbol{\varepsilon}}(t)$ is such that:

$$\overline{\boldsymbol{\varepsilon}}(t) = \mathbf{0} \quad t < 0, \quad \overline{\boldsymbol{\varepsilon}}(t) = \overline{\boldsymbol{\varepsilon}}_0 + t\dot{\overline{\boldsymbol{\varepsilon}}} \quad t \geq 0, \tag{31}$$

with an overall constant (in time) strain-rate $\dot{\overline{\boldsymbol{\varepsilon}}}$. The instantaneous response of the composite is purely elastic, that is:

$$\lim_{t\to 0^+} \boldsymbol{\sigma}(\boldsymbol{x}, t) = \boldsymbol{\sigma}_e(\boldsymbol{x}), \quad \lim_{t\to 0^+} \boldsymbol{\varepsilon}(\boldsymbol{x}, t) = \boldsymbol{\varepsilon}_e(\boldsymbol{x}) \tag{32}$$

where $(\boldsymbol{\sigma}_e, \boldsymbol{\varepsilon}_e)$ is the solution of the elastic problem

$$\boldsymbol{\varepsilon}_e(\boldsymbol{x}) = \frac{1}{2}\left(\boldsymbol{\nabla}\boldsymbol{u}_e + \boldsymbol{\nabla}\boldsymbol{u}_e^{\mathrm{T}}\right) = \boldsymbol{M}_e(\boldsymbol{x}) : \boldsymbol{\sigma}_e(\boldsymbol{x}),\ \mathrm{div}\ \boldsymbol{\sigma}_e = \mathbf{0},\ \langle \boldsymbol{\varepsilon}_e \rangle = \overline{\boldsymbol{\varepsilon}}_0. \tag{33}$$

On the other hand, the delayed response of the composite is purely viscous:

$$\lim_{t\to +\infty} \boldsymbol{\sigma}(\boldsymbol{x}, t) = \boldsymbol{\sigma}_v(\boldsymbol{x}), \quad \lim_{t\to +\infty} \dot{\boldsymbol{\varepsilon}}(\boldsymbol{x}, t) = \dot{\boldsymbol{\varepsilon}}_v(\boldsymbol{x}), \tag{34}$$

where $(\boldsymbol{\sigma}_v, \boldsymbol{\varepsilon}_v)$ is the solution of the viscous problem

$$\dot{\boldsymbol{\varepsilon}}_v(\boldsymbol{x}) = \frac{1}{2}\left(\boldsymbol{\nabla}\dot{\boldsymbol{u}}_v + \boldsymbol{\nabla}\dot{\boldsymbol{u}}_v^{\mathrm{T}}\right) = \boldsymbol{M}_v(\boldsymbol{x}) : \boldsymbol{\sigma}_v(\boldsymbol{x}),\ \mathrm{div}\ \boldsymbol{\sigma}_v = \mathbf{0},\ \langle \dot{\boldsymbol{\varepsilon}}_v \rangle = \dot{\overline{\boldsymbol{\varepsilon}}}. \tag{35}$$

The volume averages of the strain and strain-rate fields in (33) and (35) yield two classical asymptotic results for the overall response of the composite at short and large times:

$$\lim_{t\to 0^+} \overline{\boldsymbol{\sigma}}(t) = \widetilde{\boldsymbol{L}}_e : \overline{\boldsymbol{\varepsilon}}_0 \quad \text{and} \quad \lim_{t\to +\infty} \overline{\boldsymbol{\sigma}}(t) = \widetilde{\boldsymbol{L}}_v : \dot{\overline{\boldsymbol{\varepsilon}}}. \tag{36}$$

Furthermore, two new asymptotic relations can be derived (see proof in Appendix C):

$$\lim_{t\to 0^+} \dot{\overline{\boldsymbol{\sigma}}}(t) : \overline{\boldsymbol{\varepsilon}}_0 = \dot{\overline{\boldsymbol{\varepsilon}}} : \widetilde{\boldsymbol{L}}_e : \overline{\boldsymbol{\varepsilon}}_0 - \langle \boldsymbol{\sigma}_e : \boldsymbol{M}_v : \boldsymbol{\sigma}_e \rangle \tag{37}$$

and

$$\dot{\overline{\boldsymbol{\varepsilon}}} : \int_0^{+\infty} \left(\overline{\boldsymbol{\sigma}}(t) - \overline{\boldsymbol{\sigma}}_v\right)\, \mathrm{d}t = \overline{\boldsymbol{\varepsilon}}_0 : \widetilde{\boldsymbol{L}}_v : \dot{\overline{\boldsymbol{\varepsilon}}} - \langle \boldsymbol{\sigma}_v : \boldsymbol{M}_e : \boldsymbol{\sigma}_v \rangle\ . \tag{38}$$

The four asymptotic results (36), (37) and (38) imply the following relations for the effective relaxation function $\widetilde{\boldsymbol{L}}$ and the effective relaxation spectrum $\widetilde{\boldsymbol{G}}$:

$$\widetilde{\boldsymbol{L}}(0) = \int_0^{+\infty} \widetilde{\boldsymbol{G}}(\tau)\, \mathrm{d}\tau = \widetilde{\boldsymbol{L}}_e, \tag{39}$$

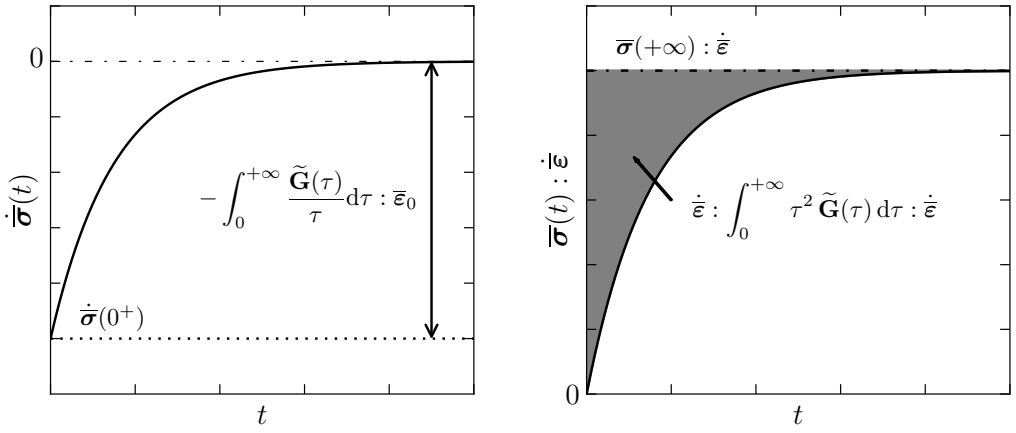

Figure 2: Interpretation of the long memory term in the overall relaxation kernel. Relaxation stress-rate for a constant applied macroscopic strain $\overline{\boldsymbol{\varepsilon}}_0$ (left) and stress response for a constant applied macroscopic strain rate $\dot{\overline{\boldsymbol{\varepsilon}}}$ (right). Exact response (solid line) and Maxwellian approximation (dot-dashed line).

$$\int_0^{+\infty} \widetilde{\boldsymbol{L}}(t) \, \mathrm{d}t = \int_0^{+\infty} \tau \, \widetilde{\boldsymbol{G}}(\tau) \, \mathrm{d}\tau = \widetilde{\boldsymbol{L}}_v, \tag{40}$$

$$\overline{\boldsymbol{\varepsilon}}_0 : \int_0^{+\infty} \frac{\widetilde{\boldsymbol{G}}(\tau)}{\tau} \, \mathrm{d}\tau : \overline{\boldsymbol{\varepsilon}}_0 = \langle \boldsymbol{\sigma}_e : \boldsymbol{M}_v : \boldsymbol{\sigma}_e \rangle \, , \tag{41}$$

$$\dot{\overline{\boldsymbol{\varepsilon}}} : \int_0^{+\infty} \tau^2 \, \widetilde{\boldsymbol{G}}(\tau) \, \mathrm{d}\tau : \dot{\overline{\boldsymbol{\varepsilon}}} = \langle \boldsymbol{\sigma}_v : \boldsymbol{M}_e : \boldsymbol{\sigma}_v \rangle \, . \tag{42}$$

The interpretation of relation (41) goes as follows: when the composite is subjected to a relaxation test ($\dot{\overline{\boldsymbol{\varepsilon}}} = \mathbf{0}$, $\overline{\boldsymbol{\varepsilon}}(t) = \overline{\boldsymbol{\varepsilon}}_0$), the limit of the macroscopic stress-rate $\dot{\overline{\boldsymbol{\sigma}}}(t) = \dot{\widetilde{\boldsymbol{L}}} : \overline{\boldsymbol{\varepsilon}}_0$ as $t \to 0^+$ is, according to (29) and (30),

$$\dot{\overline{\boldsymbol{\sigma}}}(0^+) = -\int_0^{+\infty} \frac{\widetilde{\boldsymbol{G}}(\tau)}{\tau} \, \mathrm{d}\tau : \overline{\boldsymbol{\varepsilon}}_0 \tag{43}$$

As for relation (42), when the composite is subjected to a loading at constant strain-rate ($\overline{\boldsymbol{\varepsilon}}_0 = \mathbf{0}$, $\dot{\overline{\boldsymbol{\varepsilon}}}(t) = \dot{\overline{\boldsymbol{\varepsilon}}}$), the difference between the energy dissipated in the Maxwellian approximation ($\overline{\boldsymbol{\sigma}}(+\infty) : \dot{\overline{\boldsymbol{\varepsilon}}} \, t$) and the energy dissipated in the actual composite is

$$\dot{\overline{\boldsymbol{\varepsilon}}} : \int_0^{+\infty} \tau^2 \, \widetilde{\boldsymbol{G}}(\tau) \, \mathrm{d}\tau : \dot{\overline{\boldsymbol{\varepsilon}}}. \tag{44}$$

3. Relations in Laplace space

A common practice when dealing with viscoelastic materials is to work in the Laplace domain, or in the frequency domain, rather than in the time domain. The frequency domain is particularly useful to investigate the steady-state harmonic regime of the material subjected to a periodic (in time) loading. The above asymptotic relations can be expressed in both Laplace and frequency domains.

3.1. Asymptotic relations in Laplace space

The local problem (7) can be transformed by means of the Laplace-Carson (LC) transform (Appendix A). The compatibility conditions and the equilibrium equations are unchanged, whereas the constitutive relation (5) becomes

$$p\boldsymbol{\varepsilon}^*(\boldsymbol{x},p) = (p\boldsymbol{M}_e(\boldsymbol{x}) + \boldsymbol{M}_v(\boldsymbol{x})) : \boldsymbol{\sigma}^*(\boldsymbol{x},p),\ \forall \boldsymbol{x} \in V, \tag{45}$$

where p is the Laplace parameter which is a complex number, $\boldsymbol{\varepsilon}^*$ and $\boldsymbol{\sigma}^*$ are the LC transforms of $\boldsymbol{\varepsilon}$ and $\boldsymbol{\sigma}$. Two equivalent writings of the constitutive relation of the phases are introduced favoring either elasticity or viscosity. The "elastic" formulation relates $\boldsymbol{\varepsilon}^*$ to $\boldsymbol{\sigma}^*$:

$$\boldsymbol{\varepsilon}^*(\boldsymbol{x},p) = \boldsymbol{M}^*(\boldsymbol{x},p) : \boldsymbol{\sigma}^*(\boldsymbol{x},p),$$

with

$$\boldsymbol{M}^*(\boldsymbol{x},p) = \boldsymbol{M}_e(\boldsymbol{x}) + \frac{1}{p}\boldsymbol{M}_v(\boldsymbol{x}), \tag{46}$$

whereas the "viscous" formulation relates $\dot{\boldsymbol{\varepsilon}}^*(\boldsymbol{x},p) = p\boldsymbol{\varepsilon}^*(\boldsymbol{x},p)$ to $\boldsymbol{\sigma}^*$:

$$\dot{\boldsymbol{\varepsilon}}^*(\boldsymbol{x},p) = \boldsymbol{\mathcal{M}}^*(\boldsymbol{x},p) : \boldsymbol{\sigma}^*(\boldsymbol{x},p),$$

with

$$\boldsymbol{\mathcal{M}}^*(\boldsymbol{x},p) = p\,\boldsymbol{M}^*(\boldsymbol{x},p) = p\boldsymbol{M}_e(\boldsymbol{x}) + \boldsymbol{M}_v(\boldsymbol{x}). \tag{47}$$

The effective constitutive relations in LC space read equivalently

$$\overline{\boldsymbol{\varepsilon}}^*(p) = \widetilde{\boldsymbol{M}}^*(p) : \overline{\boldsymbol{\sigma}}^*(p) \quad \text{or} \quad \dot{\overline{\boldsymbol{\varepsilon}}}^*(p) = \widetilde{\boldsymbol{\mathcal{M}}}^*(p) : \overline{\boldsymbol{\sigma}}^*(p), \tag{48}$$

where $\widetilde{\boldsymbol{M}}^*(p)$ is related to the effective spectrum $\widetilde{\boldsymbol{J}}$ through:

$$\widetilde{\boldsymbol{M}}^*(p) = \widetilde{\boldsymbol{M}}_e + \frac{1}{p}\widetilde{\boldsymbol{M}}_v + \int_0^{+\infty} \frac{\widetilde{\boldsymbol{J}}(\tau)}{1+p\tau}\,\mathrm{d}\tau, \tag{49}$$

and $\widetilde{\boldsymbol{\mathcal{M}}}^*(p) = p\widetilde{\boldsymbol{M}}^*(p)$.

In this section, counterparts in Laplace space to the relations (18), (19), (27) and (28) are established. By making use of the initial and final value theorems (see Appendix A), it is immediately found that

$$\lim_{p\to+\infty} \widetilde{\boldsymbol{M}}^*(p) = \widetilde{\boldsymbol{M}}_e, \tag{50}$$

and

$$\lim_{p\to 0} \widetilde{\boldsymbol{\mathcal{M}}}^*(p) = \widetilde{\boldsymbol{M}}_v, \tag{51}$$

which are the counterparts of (18) and (19) respectively. The counterparts of relations (27) and (28) in Laplace space are:

$$\lim_{p\to+\infty} \overline{\boldsymbol{\sigma}} : \frac{\partial \widetilde{\boldsymbol{M}}^*}{\partial(1/p)}(p) : \overline{\boldsymbol{\sigma}} = \langle \boldsymbol{\sigma}_e : \boldsymbol{M}_v : \boldsymbol{\sigma}_e \rangle \,, \tag{52}$$

and

$$\overline{\boldsymbol{\sigma}} : \frac{\partial \widetilde{\boldsymbol{\mathcal{M}}}^*}{\partial p}(0) : \overline{\boldsymbol{\sigma}} = \langle \boldsymbol{\sigma}_v : \boldsymbol{M}_e : \boldsymbol{\sigma}_v \rangle \tag{53}$$

where $\boldsymbol{\sigma}_e$ and $\boldsymbol{\sigma}_v$ are the solutions of the purely elastic problem (13) and purely viscous problem (15).

A direct derivation of these relations, independent from (20) and (21), is given in Appendix D through a study of the asymptotic behavior of $\widetilde{\boldsymbol{M}}^*(p)$ and $\widetilde{\boldsymbol{\mathcal{M}}}^*(p)$ in Laplace space for small and large p's, as was done for the relaxation function in Suquet (2012). A different proof is given here showing how (52) and (53) follow from (20) and (21) respectively.

It follows from (A.6) that

$$\lim_{t\to 0^+} \overline{\boldsymbol{\sigma}} : \dot{\overline{\boldsymbol{\varepsilon}}} = \lim_{p\to+\infty} p\, \overline{\boldsymbol{\sigma}} : (\overline{\boldsymbol{\varepsilon}}^*(p) - \overline{\boldsymbol{\varepsilon}}(0)) = \lim_{p\to+\infty} p\, \overline{\boldsymbol{\sigma}} : \left(\widetilde{\boldsymbol{M}}^*(p) - \widetilde{\boldsymbol{M}}(0)\right) : \overline{\boldsymbol{\sigma}}.$$

The last term is evaluated by setting $q = 1/p$:

$$\lim_{p\to+\infty} p\, \overline{\boldsymbol{\sigma}} : \left(\widetilde{\boldsymbol{M}}^*(p) - \widetilde{\boldsymbol{M}}(0)\right) : \overline{\boldsymbol{\sigma}} = \lim_{q\to 0} \overline{\boldsymbol{\sigma}} : \frac{\widetilde{\boldsymbol{M}}^*(q) - \widetilde{\boldsymbol{M}}^*(q=0)}{q} : \overline{\boldsymbol{\sigma}},$$

where the initial and final value theorem has been used to obtain

$$\widetilde{\boldsymbol{M}}(0) = \lim_{p\to+\infty} \widetilde{\boldsymbol{M}}^*(p) = \lim_{q\to 0} \widetilde{\boldsymbol{M}}^*(q).$$

It is then found that

$$\lim_{t\to 0^+} \overline{\boldsymbol{\sigma}} : \dot{\overline{\boldsymbol{\varepsilon}}} = \overline{\boldsymbol{\sigma}} : \frac{\partial \widetilde{\boldsymbol{M}}^*}{\partial q}(q=0) : \overline{\boldsymbol{\sigma}} = \lim_{p\to+\infty} \overline{\boldsymbol{\sigma}} : \frac{\partial \widetilde{\boldsymbol{M}}^*}{\partial (1/p)}(p) : \overline{\boldsymbol{\sigma}}. \tag{54}$$

Equation (52) results from (54) and (20). As for relation (53), it is noted with the help of (A.6) that

$$\begin{aligned}
&\lim_{t\to+\infty} \overline{\boldsymbol{\sigma}} : (\overline{\boldsymbol{\varepsilon}}(t) - \overline{\boldsymbol{\varepsilon}}^{Maxw}(t)) = \lim_{p\to 0} \overline{\boldsymbol{\sigma}} : (\overline{\boldsymbol{\varepsilon}}^*(p) - (\overline{\boldsymbol{\varepsilon}}^{Maxw})^*(p)) \\
&= \lim_{p\to 0} \overline{\boldsymbol{\sigma}} : (\widetilde{\boldsymbol{M}}^*(p) - \widetilde{\boldsymbol{M}}_e - \frac{1}{p}\widetilde{\boldsymbol{M}}_v) : \overline{\boldsymbol{\sigma}} = \lim_{p\to 0} \left(\overline{\boldsymbol{\sigma}} : \frac{\widetilde{\boldsymbol{\mathcal{M}}}^*(p) - \widetilde{\boldsymbol{M}}_v}{p} : \overline{\boldsymbol{\sigma}} \right) - \overline{\boldsymbol{\sigma}} : \widetilde{\boldsymbol{M}}_e : \overline{\boldsymbol{\sigma}} \\
&= \overline{\boldsymbol{\sigma}} : \frac{\partial \widetilde{\boldsymbol{\mathcal{M}}}^*}{\partial p}(0) : \overline{\boldsymbol{\sigma}} - \overline{\boldsymbol{\sigma}} : \widetilde{\boldsymbol{M}}_e : \overline{\boldsymbol{\sigma}}.
\end{aligned} \tag{55}$$

Equation (53) results from (55) and (21).

3.2. Asymptotic relations in frequency domain

The above relations (50), (51), (52), and (53) are valid even when p is a purely imaginary number. The response of the composite to a periodic loading is classically studied in the frequency domain by taking $p = \imath\omega$, where $\imath = \sqrt{-1}$ and ω is the frequency. The macroscopic harmonic loading reads

$$\overline{\boldsymbol{\sigma}}(t) = \overline{\boldsymbol{\sigma}}^* \, \mathrm{e}^{\imath\omega t} \quad \text{or} \quad \overline{\boldsymbol{\varepsilon}}(t) = \overline{\boldsymbol{\varepsilon}}^* \, \mathrm{e}^{\imath\omega t}. \tag{56}$$

Asymptotic relations in the frequency domain are obtained from (50), (51), (52), and (53) (the proof is omitted here for conciseness):

$$\left.\begin{aligned}
\lim_{\omega\to+\infty} \widetilde{\boldsymbol{M}}^*(\imath\omega) &= \widetilde{\boldsymbol{M}}_e, \\
\lim_{\omega\to 0} \widetilde{\boldsymbol{\mathcal{M}}}^*(\imath\omega) &= \widetilde{\boldsymbol{M}}_v, \\
\lim_{\omega\to+\infty} -\imath\,\omega^2 \overline{\boldsymbol{\sigma}}^* : \frac{\partial \widetilde{\boldsymbol{M}}^*}{\partial \omega}(\imath\omega) : \overline{\boldsymbol{\sigma}}^* &= \langle \boldsymbol{\sigma}_e : \boldsymbol{M}_v : \boldsymbol{\sigma}_e \rangle \,, \\
\lim_{\omega\to 0} -\imath\,\overline{\boldsymbol{\sigma}}^* : \frac{\partial \widetilde{\boldsymbol{\mathcal{M}}}^*}{\partial \omega}(\imath\omega) : \overline{\boldsymbol{\sigma}}^* &= \langle \boldsymbol{\sigma}_v : \boldsymbol{M}_e : \boldsymbol{\sigma}_v \rangle \,,
\end{aligned}\right\} \tag{57}$$

Note that $\widetilde{\boldsymbol{M}}^*(\imath\omega)$ and $\widetilde{\boldsymbol{\mathcal{M}}}^*(\imath\omega)$ are complex and therefore that the left-hand-side of (57) is complex, whereas its right-hand-side is real. It is convenient to

express these relations in terms of the *storage moduli* $\widetilde{\boldsymbol{L}}'(\omega)$ and *loss moduli* $\widetilde{\boldsymbol{L}}''(\omega)$ defined as the real and imaginary parts of the complex stiffness tensor $\widetilde{\boldsymbol{L}}^*(\imath\omega)$:

$$\widetilde{\boldsymbol{L}}^*(\imath\omega) = \widetilde{\boldsymbol{L}}'(\omega) + \imath\widetilde{\boldsymbol{L}}''(\omega).$$

Asymptotic relations can be deduced from (57) for the storage and loss moduli:

$$\left.\begin{array}{c} \lim\limits_{\omega\to+\infty} \widetilde{\boldsymbol{L}}'(\omega) = \widetilde{\boldsymbol{L}}_e, \quad \lim\limits_{\omega\to+\infty} \widetilde{\boldsymbol{L}}''(\omega) = \boldsymbol{0} \\ \lim\limits_{\omega\to 0} \dfrac{1}{\omega}\widetilde{\boldsymbol{L}}'(\omega) = \boldsymbol{0}, \quad \lim\limits_{\omega\to 0} \dfrac{1}{\omega}\widetilde{\boldsymbol{L}}''(\omega) = \widetilde{\boldsymbol{L}}_v \\ \lim\limits_{\omega\to+\infty} -\omega^2\overline{\boldsymbol{\varepsilon}}^* : \dfrac{\partial\widetilde{\boldsymbol{L}}'}{\partial\omega}(\omega) : \overline{\boldsymbol{\varepsilon}}^* = 0, \quad \lim\limits_{\omega\to+\infty} -\omega^2\overline{\boldsymbol{\varepsilon}}^* : \dfrac{\partial\widetilde{\boldsymbol{L}}''}{\partial\omega}(\omega) : \overline{\boldsymbol{\varepsilon}}^* = \langle \boldsymbol{\sigma}_e : \boldsymbol{M}_v : \boldsymbol{\sigma}_e \rangle \,, \\ \lim\limits_{\omega\to 0} \overline{\boldsymbol{\varepsilon}}^* : \dfrac{\partial}{\partial\omega}\left(\dfrac{1}{\omega}\widetilde{\boldsymbol{L}}'(\omega)\right) : \overline{\boldsymbol{\varepsilon}}^* = \langle \boldsymbol{\sigma}_v : \boldsymbol{M}_e : \boldsymbol{\sigma}_v \rangle \,, \quad \lim\limits_{\omega\to 0} \overline{\boldsymbol{\varepsilon}}^* : \dfrac{\partial}{\partial\omega}\left(\dfrac{1}{\omega}\widetilde{\boldsymbol{L}}''(\omega)\right) : \overline{\boldsymbol{\varepsilon}}^* = 0, \end{array}\right\} \tag{58}$$

These asymptotic relations can be further specialized when the phases are incompressible and expressed in terms of the usual storage and loss shear moduli $G'(\omega)$ and $G''(\omega)$.

4. An approximate model based on Prony series

4.1. Restrictions on Prony series

In the absence of expressions for the relaxation spectrum $\widetilde{\boldsymbol{G}}$ or the retardation spectrum $\widetilde{\boldsymbol{J}}$ in closed forms, a common practice is to approximate them by a box function or by a sum of delta functions (Eyre et al., 2002). In the latter case, the effective relaxation kernel $\widetilde{\boldsymbol{L}}(t)$ is approximated by a sum of exponentials (Prony series) corresponding to the relaxation kernel of a generalized Maxwell model, *i.e.* Maxwell elements arranged in a parallel fashion (Christensen, 1971):

$$\widetilde{\boldsymbol{L}}(t) \simeq \widetilde{\boldsymbol{L}}_{Prony}(t) = \sum_{i=1}^{M} \overline{\boldsymbol{L}}_i \, \mathrm{e}^{-t/\overline{\tau}_i}. \tag{59}$$

For simplicity each term in the series (59) is associated with a single relaxation time $\overline{\tau}_i$ but the tensors $\overline{\boldsymbol{L}}_i$ can be fully anisotropic. However, the present results apply to more general situations as will be illustrated below (see also Vu et al., 2012, Appendix A).

The LC transform of the relaxation function (59) can be expressed as

$$\widetilde{\boldsymbol{L}}^*(p) = p\widetilde{\boldsymbol{\mathcal{L}}}^*(p) \simeq \sum_{i=1}^{M} \frac{p}{\left(p + \dfrac{1}{\overline{\tau}_i}\right)} \overline{\boldsymbol{L}}_i = \frac{p\,\boldsymbol{Q}(p)}{\displaystyle\prod_{i=1}^{M}\left(p + \frac{1}{\overline{\tau}_i}\right)} \tag{60}$$

where $\boldsymbol{Q}(p)$ is a (tensorial) polynom of degree $M-1$ in p. Note that when the complex number p is taken to be purely imaginary, in the form $p = \imath\omega$, equation (60) provides an approximation of the effective storage and loss moduli describing the harmonic steady-state response of the composite at frequency ω :

$$\widetilde{\boldsymbol{L}}'(\omega) \simeq \sum_{i=1}^{M} \overline{\boldsymbol{L}}_i \frac{{\overline{\tau}_i}^2\omega^2}{1 + {\overline{\tau}_i}^2\omega^2} \quad \text{and} \quad \widetilde{\boldsymbol{L}}''(\omega) \simeq \sum_{i=1}^{M} \overline{\boldsymbol{L}}_i \frac{\overline{\tau}_i\omega}{1 + {\overline{\tau}_i}^2\omega^2}. \tag{61}$$

Under the approximation (60), the LC transform $\widetilde{\boldsymbol{M}}^*(p)$ of the creep function satisfying $\widetilde{\boldsymbol{M}}^*(p) : \widetilde{\boldsymbol{L}}^*(p) = \boldsymbol{I}$, reads

$$\widetilde{\boldsymbol{M}}^*(p) = \frac{1}{p}\widetilde{\boldsymbol{\mathcal{M}}}^*(p) \simeq \widetilde{\boldsymbol{M}}^*_{Prony}(p) = \frac{1}{p}\prod_{i=1}^{M}\left(p + \frac{1}{\overline{\tau}_i}\right)\boldsymbol{Q}^{-1}(p). \tag{62}$$

$\widetilde{\boldsymbol{M}}^*_{Prony}(p)$ can alternatively be put in the form:

$$\widetilde{\boldsymbol{M}}^*_{Prony}(p) \simeq \widetilde{\boldsymbol{M}}_0 + \frac{1}{p}\widetilde{\boldsymbol{M}}_\infty + \sum_{i=1}^{M-1} \frac{1}{1 + \overline{\theta}_i p}\overline{\boldsymbol{M}}_i, \tag{63}$$

where the creep parameters $\widetilde{\boldsymbol{M}}_0$, $\widetilde{\boldsymbol{M}}_\infty$, $\overline{\boldsymbol{M}}_i$ and $\overline{\theta}_i$ are related to the relaxation parameters $\overline{\boldsymbol{L}}_i$ and $\overline{\tau}_i$ through relations which will not be given here except when $M = 2$ (see relations (70)). The creep function is thus approximated as

$$\widetilde{\boldsymbol{M}}(t) \simeq \widetilde{\boldsymbol{M}}_{Prony}(t) = \widetilde{\boldsymbol{M}}_0 + t\,\widetilde{\boldsymbol{M}}_\infty + \sum_{i=1}^{M-1} \overline{\boldsymbol{M}}_i\,(1 - \mathrm{e}^{-t/\overline{\theta}_i}). \tag{64}$$

This creep function corresponds to a generalized Kelvin-Voigt model combining a Maxwell model in parallel with $M-1$ Kelvin-Voigt models connected

in series, which is the *conjugate model* of the generalized Maxwell model introduced in (59) (Tschoegl, 1989). The conjugate models (59) and (64) are strictly equivalent (*i.e.* for a given loading history, they deliver the same response) and lead to dual formulations of the composite's response by internal variables (Appendix E).

The asymptotic relations (50), (51), (52) and (53) on the LC transform of the effective overall creep function provide restrictions on the approximation (64):

$$\left.\begin{array}{rcl} \widetilde{\boldsymbol{M}}_0 &=& \widetilde{\boldsymbol{M}}_e, \\ \widetilde{\boldsymbol{M}}_\infty &=& \widetilde{\boldsymbol{M}}_v, \\ \overline{\boldsymbol{\sigma}} : \left(\widetilde{\boldsymbol{M}}_\infty + \displaystyle\sum_{i=1}^{M-1} \frac{1}{\overline{\theta}_i} \overline{\boldsymbol{M}}_i \right) : \overline{\boldsymbol{\sigma}} &=& \displaystyle\sum_r c^{(r)}\, \boldsymbol{M}_v^{(r)} :: \langle \boldsymbol{\sigma}_e \otimes \boldsymbol{\sigma}_e \rangle^{(r)}, \\ \overline{\boldsymbol{\sigma}} : \left(\widetilde{\boldsymbol{M}}_0 + \displaystyle\sum_{i=1}^{M-1} \overline{\boldsymbol{M}}_i \right) : \overline{\boldsymbol{\sigma}} &=& \displaystyle\sum_r c^{(r)}\, \boldsymbol{M}_e^{(r)} :: \langle \boldsymbol{\sigma}_v \otimes \boldsymbol{\sigma}_v \rangle^{(r)}. \end{array}\right\} \quad (65)$$

The first two equations are well-known, the last two equations are new (dual of the relations of Suquet (2012)). These equations are scalar or tensorial depending on the class of isotropy of the phases and of the composite itself. This set of four conditions on the Prony series can be used to determine a minimal approximation with four parameters (scalar or tensorial), improving on the Maxwellian approximation which makes use only of the first two equations in (65).

4.2. Approximate model for isotropic composites

The tensorial conditions (65) are now specified for composites presenting macroscopic isotropy. Their overall creep function may thus be written as

$$\widetilde{\boldsymbol{M}}(t) = \widetilde{M}^{(m)}(t)\boldsymbol{J} + \widetilde{M}^{(d)}(t)\boldsymbol{K} \simeq \widetilde{M}^{(m)}_{Prony}(t)\boldsymbol{J} + \widetilde{M}^{(d)}_{Prony}(t)\boldsymbol{K}, \quad (66)$$

with

$$\left.\begin{array}{l} \widetilde{M}^{(m)}_{Prony}(t) = \widetilde{M}^{(m)}_0 + t\, \widetilde{M}^{(m)}_\infty + \displaystyle\sum_{i=1}^{M-1} \overline{M}^{(m)}_i \, (1 - \mathrm{e}^{-t/\overline{\theta}^{(m)}_i}), \\ \widetilde{M}^{(d)}_{Prony}(t) = \widetilde{M}^{(d)}_0 + t\, \widetilde{M}^{(d)}_\infty + \displaystyle\sum_{i=1}^{M-1} \overline{M}^{(d)}_i \, (1 - \mathrm{e}^{-t/\overline{\theta}^{(d)}_i}). \end{array}\right\} \quad (67)$$

$\boldsymbol{J}$ and $\boldsymbol{K}$ denote the projectors on hydrostatic and traceless symmetric second-order tensors and the components on each tensorial subspace are respectively indicated by superscripts (m) and (d). The set of relations (65) becomes

$$\left.\begin{array}{rcl}
\widetilde{M}_0^{(m)} = \widetilde{M}_e^{(m)}, \quad \widetilde{M}_0^{(d)} = \widetilde{M}_e^{(d)}, \qquad \widetilde{M}_\infty^{(m)} = \widetilde{M}_v^{(m)}, \quad \widetilde{M}_\infty^{(d)} = \widetilde{M}_v^{(d)}, & & \\
\left(\widetilde{M}_\infty^{(d)} + \displaystyle\sum_{i=1}^{M-1} \frac{\overline{M}_i^{(d)}}{\overline{\theta}_i^{(d)}}\right) \overline{\boldsymbol{s}} : \overline{\boldsymbol{s}} & = & \displaystyle\sum_r \boldsymbol{M}_v^{(r)} :: \left(\overline{\boldsymbol{s}} : \frac{\partial \widetilde{\boldsymbol{M}}_e}{\partial \boldsymbol{M}_e^{(r)}} : \overline{\boldsymbol{s}}\right), \\
\left(\widetilde{M}_0^{(d)} + \displaystyle\sum_{i=1}^{M-1} \overline{M}_i^{(d)}\right) \overline{\boldsymbol{s}} : \overline{\boldsymbol{s}} & = & \displaystyle\sum_r \boldsymbol{M}_e^{r} :: \left(\overline{\boldsymbol{s}} : \frac{\partial \widetilde{\boldsymbol{M}}_v}{\partial \boldsymbol{M}_v^{(r)}} : \overline{\boldsymbol{s}}\right), \\
\left(\widetilde{M}_\infty^{(m)} + \displaystyle\sum_{i=1}^{M-1} \frac{\overline{M}_i^{(m)}}{\overline{\theta}_i^{(m)}}\right) \overline{\boldsymbol{p}} : \overline{\boldsymbol{p}} & = & \displaystyle\sum_r \boldsymbol{M}_v^{(r)} :: \left(\overline{\boldsymbol{p}} : \frac{\partial \widetilde{\boldsymbol{M}}_e}{\partial \boldsymbol{M}_e^{(r)}} : \overline{\boldsymbol{p}}\right), \\
\left(\widetilde{M}_0^{(m)} + \displaystyle\sum_{i=1}^{M-1} \overline{M}_i^{(m)}\right) \overline{\boldsymbol{p}} : \overline{\boldsymbol{p}} & = & \displaystyle\sum_r \boldsymbol{M}_e^{r} :: \left(\overline{\boldsymbol{p}} : \frac{\partial \widetilde{\boldsymbol{M}}_v}{\partial \boldsymbol{M}_v^{(r)}} : \overline{\boldsymbol{p}}\right)
\end{array}\right\} \tag{68}$$

where $\overline{\boldsymbol{s}}$ and $\overline{\boldsymbol{p}}$ denote purely deviatoric and hydrostatic macroscopic stress tensors.

The four relations in the first line of (68) define the Maxwellian component of the creep function. The last four relations, which impose conditions on the $4(M-1)$ parameters $\left(\overline{M}_i^{(m)}, \overline{M}_i^{(d)}, \overline{\theta}_i^{(m)}, \overline{\theta}_i^{(d)}\right)$, are not sufficient to determine them all, except when $M = 2$, *i.e.* when the approximation (59) involves only two terms or, equivalently, when the expansion (64) has a third term in addition to the two first terms forming the Maxwellian approximation. In this approximation $M = 2$, the independent unknowns $\left(\overline{M}_1^{(m)}, \overline{M}_1^{(d)}, \overline{\theta}_1^{(m)}, \overline{\theta}_1^{(d)}\right)$ can be identified from the last four relations (68) and the approximate model is fully determined by the asymptotic relations. The approximation (67) with $M = 2$ consists in approaching each component of the effective retardation spectrum $\widetilde{\boldsymbol{J}}$ by single Dirac functions, respectively at $\tau = \overline{\theta}_1^{(m)}$ and $\tau = \overline{\theta}_1^{(d)}$:

$$\widetilde{\boldsymbol{J}}(\tau) \simeq \overline{M}_1^{(m)} \delta_{\overline{\theta}_1^{(m)}}(\tau) \boldsymbol{J} + \overline{M}_1^{(d)} \delta_{\overline{\theta}_1^{(d)}}(\tau) \boldsymbol{K}. \tag{69}$$

Furthermore, when $M = 2$, the parameters of the conjugate models (59) and

(64) are related through

$$\overline{\theta}_1^{(q)} = \frac{\overline{\tau}_1^{(q)}\overline{\tau}_2^{(q)}\widetilde{M}_v^{(q)}}{\widetilde{M}_e^{(q)}} \quad \text{and} \quad \overline{M}_1^{(q)} = \widetilde{M}_e^{(q)}\,(\widetilde{M}_v^{(q)})^2\,\overline{L}_1^{(q)}\,\overline{L}_2^{(q)}\,(\overline{\tau}_1^{(q)} - \overline{\tau}_2^{(q)})^2 \quad (70)$$

with $q = m, d$.

Remark: The interpretation of the integrals $\displaystyle\int_0^{+\infty} \widetilde{\boldsymbol{J}}(\tau)\,\mathrm{d}\tau$ and $\displaystyle\int_0^{+\infty} \frac{\widetilde{\boldsymbol{J}}(\tau)}{\tau}\,\mathrm{d}\tau$ can be reformulated with this approximation as:

- $\overline{M}_1^{(m)}$ and $\overline{M}_1^{(d)}$ are the differences in the dilatational and shear strains at large time between the model (66) and the Maxwellian approximation:

$$\overline{M}_1^{(q)} = \lim_{t\to+\infty} \widetilde{M}_{Prony}^{(q)}(t) - (\widetilde{M}_e^{(q)} + t\,\widetilde{M}_v^{(q)}), \quad q = m, d$$

- The ratios $\overline{M}_1^{(m)}/\overline{\theta}_1^{(m)}$ and $\overline{M}_1^{(d)}/\overline{\theta}_1^{(d)}$ are the differences in dilatational and shear strain-rates between $t = 0$ and $t \to +\infty$ predicted by the approximate model:

$$\frac{\overline{M}_1^{(q)}}{\overline{\theta}_1^{(q)}} = \dot{\widetilde{M}}_{Prony}^{(q)}(0) - \widetilde{M}_v^{(q)}, \quad q = m, d.$$

The right-hand sides of the last four relations in (68) require the second moments of the stress field for the purely elastic and viscous problems, which will be specified in the next paragraphs depending on the microstructure of the composite.

5. Application to particulate and granular microstructures

The accuracy of the proposed model is assessed in this section by comparison with exact analytical results, when available, and with other reference results obtained either by full-field simulations performed by a method based on fast Fourier transforms (FFT) or by a mean-field method relying on the collocation method. Both methods are briefly described in the next subsections.

5.1. Reference results

5.1.1. FFT full-field computations

Full-field simulations were performed by means of the FFT method of Moulinec and Suquet (1998). This method was initially developed for linear elastic or elasto-plastic composites and extended to more general constitutive relations, including viscoelastic, elasto-viscoplastic composites with isotropic and/or kinematic hardening in Idiart et al. (2006); Suquet et al. (2012). It has also been extended from two-phase composites to polycrystals (N-phase composites) by Lebensohn (2001); Lebensohn et al. (2011, 2012); Suquet (2012).

The simulations presented below were performed with the software CraFT (Labé et al., 2011) on polycrystalline 3D microstructures. A cubic unit-cell is divided into N grains by a Voronoi tesselation ($N = 4096$ in the present study). In the most general case of untextured polycrystals (Subsection 5.5), the orientation of each individual grain is chosen randomly. For two-phase granular microstructures (Subsection 5.2), the material properties of each grain are chosen randomly to be either the properties of phase 1 or of phase 2, under the only constraint of equal volume fraction. The unit-cell is discretized into 256^3 voxels. 10 different realizations of the unit-cell are generated from different random seeds for the Voronoi tesselations and for the orientations (a typical realization is shown in Figure 3). The overall responses of the 10 different realizations are averaged. The deviation between the different realizations was observed to be small (less than 1 % in most cases) and, although no systematic study on the size of the un! it-cell, on the number of grains and on the number of realizations has been conducted in the course of the present study, our experience from previous studies (Suquet et al., 2012) is that these numbers are sufficient to ensure stationarity of the effective properties.

5.1.2. Collocation method

The collocation method (Schapery, 1962) relies on the approximation of the effective relaxation (resp. creep) function by a Prony serie (59) with an *a priori* chosen set of M relaxation times $\overline{\tau}_i$ (*i.e.* collocation points). The coefficients $\overline{\boldsymbol{L}_i}$ of the series are determined by minimizing the quadratic error between the exact function and its approximation

$$\min_{\overline{\boldsymbol{L}_i}} \int_0^{+\infty} \left(\widetilde{\boldsymbol{L}}(t) - \widetilde{\boldsymbol{L}}_{Prony}(t) \right)^2 \mathrm{d}t. \tag{71}$$

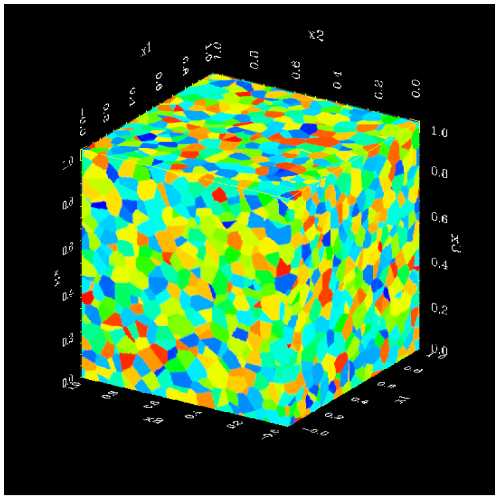

Figure 3: A typical Voronoi tesselation of the unit-cell into 4096 grains.

This minimization leads to the following collocation condition

$$\widetilde{\boldsymbol{L}}^*(\overline{p}_r) = \widetilde{\boldsymbol{L}}^*_{Prony}(\overline{p}_r) \quad \text{with} \quad \overline{p}_r = 1/\overline{\tau}_r,\ \forall r = 1, \ldots, M. \tag{72}$$

In other words, the best approximation of the exact relaxation function is obtained when its LC transform is equal to the LC transform of its Prony approximation at M collocation points $\overline{p}_r$. From a practical point of view, the method requires the computation of the LC transform $\widetilde{\boldsymbol{L}}^*(p)$ of the exact function at each collocation point. Relation (72) defines a linear system allowing for the determination of the coefficients $\overline{\boldsymbol{L}_i}$.

5.2. Granular two-phase composites

Two-phase composites made of isotropic incompressible phases with equal volume fraction and with a random granular microstructure are considered first. As is well documented, an accurate estimate of their effective response can be obtained by means of the self-consistent scheme (Suquet and Moulinec, 1997). The elastic or viscous compliance tensor of phase (r) is given by

$$\boldsymbol{M}^{(r)} = M^{(r)}\,\boldsymbol{K}, \quad M^{(r)} = \frac{1}{2\mu^{(r)}}, \quad r = 1,\, 2, \tag{73}$$

and the intraphase second moment of the stress field reads

$$\boldsymbol{K} :: \langle \boldsymbol{s} \otimes \boldsymbol{s} \rangle^{(r)} = \frac{1}{c^{(r)}} \frac{\partial \widetilde{M}}{\partial M^{(r)}}\, \overline{\boldsymbol{s}} : \overline{\boldsymbol{s}}. \tag{74}$$

Applying this relation to the elastic and viscous stress fields, one obtains from (68) the expressions of the two parameters describing the deviatoric transient viscoelastic behaviour

$$\overline{M}_1 = \sum_{r=1}^{2} M_e^{(r)} \frac{\partial \widetilde{M}_v}{\partial M_v^{(r)}} - \widetilde{M}_e \quad \text{and} \quad \frac{\overline{M}_1}{\overline{\theta}_1} = \sum_{r=1}^{2} M_v^{(r)} \frac{\partial \widetilde{M}_e}{\partial M_e^{(r)}} - \widetilde{M}_v \tag{75}$$

where the superscript (d) has been omitted for brevity. The self-consistent estimate of the effective compliance $\widetilde{M}$, is solution of the quadratic equation

$$\widetilde{M}^2 - \frac{1}{4}(M^{(1)} + M^{(2)})\widetilde{M} + \frac{3}{2} M^{(1)} M^{(2)} = 0. \tag{76}$$

Explicit expressions for the partial derivatives of $\widetilde{M}$ entering (75) are obtained by derivation of (76).

In order to check the accuracy of the approximate model, the material is subjected to the following stress loading history

$$\left.\begin{array}{l} \overline{\sigma}_{\rm eq}(t) = 1\,{\rm MPa},\ \forall t \in [0, t_1]; \\ \overline{\sigma}_{\rm eq}(t) = 3\,{\rm MPa},\ \forall t > t_1. \end{array}\right\} \tag{77}$$

with $t_1 = 2\,{\rm s}$. The predictions of the model are compared in Figure 4 with reference FFT full-field computations on 3D Voronoi tesselations containing 4096 grains, the collocation method using 5 terms in the Prony series and the Maxwellian approximation. Two sets of material data from Suquet (2012) are used, corresponding to moderate and strong contrasts between the relaxation times of the phases:

$$\text{Moderate contrast:} \quad \left.\begin{array}{l} \mu_e^{(1)} = 1\,{\rm MPa},\ \mu_v^{(1)} = 2\,{\rm MPa.s},\ \ \tau^{(1)} = 2\,{\rm s}, \\ \mu_e^{(2)} = 100\,{\rm MPa},\ \mu_v^{(2)} = 20\,{\rm MPa.s},\ \tau^{(2)} = 0.2\,{\rm s}. \end{array}\right\} \tag{78}$$

$$\text{Strong contrast:} \quad \left.\begin{array}{l} \mu_e^{(1)} = 1\,{\rm MPa},\ \mu_v^{(1)} = 5\ {\rm MPa.s},\ \tau^{(1)} = 5\,{\rm s}, \\ \mu_e^{(2)} = 50\,{\rm MPa},\ \mu_v^{(2)} = 2.5\,{\rm MPa.s},\ \tau^{(2)} = 0.05\,{\rm s}, \end{array}\right\} \tag{79}$$

where $\mu^{(r)} = 1/2M^{(r)}$ is the elastic or viscous shear modulus of the two phases. The agreement between the model, the FFT numerical scheme and the collocation method is excellent at moderate contrast (the model improves significantly on the Maxwellian approximation). It deteriorates when the

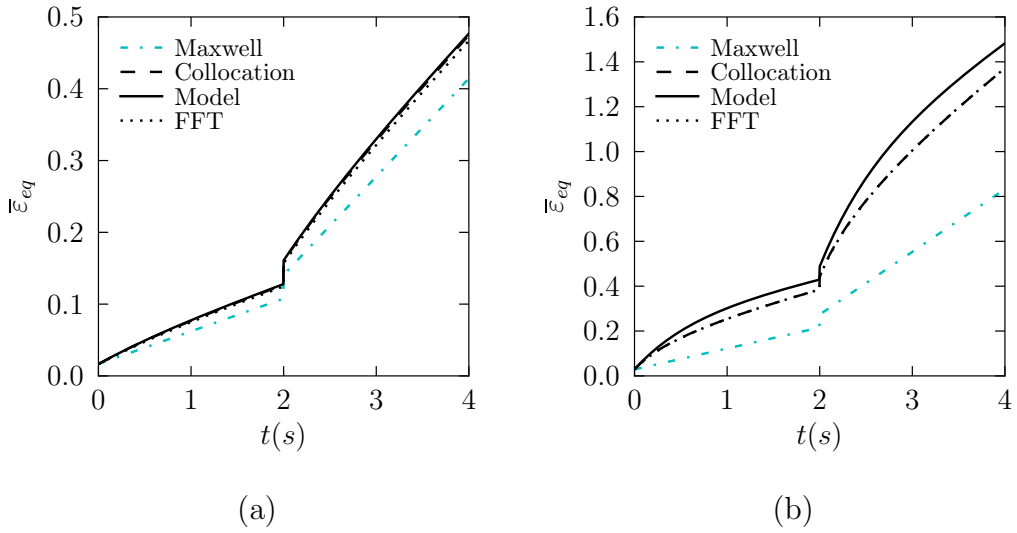

Figure 4: Isotropic two-phase composites with random microstructure. Comparison of approximations by the self-consistent estimate. (a): moderate contrast and (b) strong contrast between the retardation times of the phases.

contrast increases, as expected since the retardation spectrum of the self-consistent model is a continuous function between $\tau^{(1)}$ and $\tau^{(2)}$ (Rougier et al., 1993). This spectrum is thus poorly approximated by a single retardation time when $\tau^{(1)}$ and $\tau^{(2)}$ are far apart. Finally, it can be also noted that the agreement between the FFT and the collocation results, at both moderate and high contrast, confirms the accuracy of the collocation method, as is documented in the literature (see, for instance, Brenner et al., 2002; Rekik and Brenner, 2011; Vu et al., 2012).

5.3. Particle-reinforced two-phase composites

5.3.1. Generalized self-consistent estimate

When the composites under consideration are particle-reinforced materials where the inclusions are surrounded by a layer of matrix ("cherry-pit" microstructure), their effective linear properties can be accurately predicted by the generalized self-consistent scheme (GSC) (*i.e.* three-phase model). The GSC model, which relies on the solution for a coated inclusion embedded in an infinite medium (Christensen and Lo, 1979; Hervé and Zaoui, 1990), leads to continuous relaxation/retardation spectra, like the self-consistent scheme

(Beurthey and Zaoui, 2000). The predictions of the model of Subsection 4.2 are compared in Figure 5 with reference results. The material data and

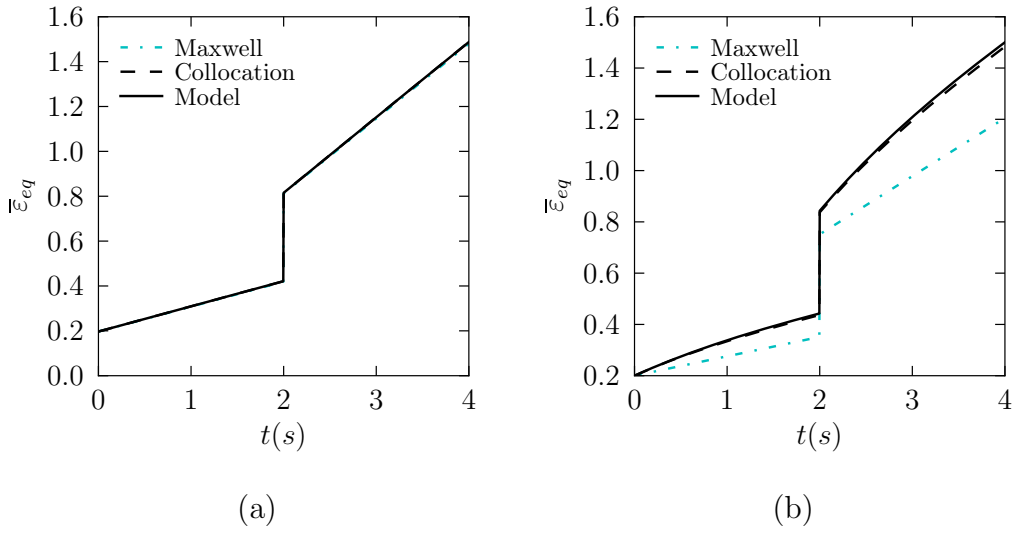

Figure 5: Isotropic two-phase composites with inclusion-matrix microstructure. Comparison of approximations by the generalized self-consistent estimate with (a) moderate contrast and (b) strong contrast. The volume fraction of the particles is $c^{(2)} = 0.2$.

the creep loading considered are identical to those used for incompressible granular two-phase composites. The particulate composite comprises 20% of inclusions. The model agrees very well with reference collocation results for both moderate and high contrasts in the phase relaxation times. In the case of a moderate contrast, the overall response is almost Maxwellian.

5.3.2. Hashin-Shtrikman estimate

Another relevant estimate for reinforced particulate composites is the Hashin-Shtrikman lower bound (when the inclusions are stiffer than the matrix) with the matrix as reference medium. By contrast with the generalized self-consistent estimate, it is known that the effective relaxation spectrum of composites attaining the Hashin-Shtrikman bound consists of discrete Dirac masses (Ricaud and Masson, 2009). To pursue the assessment of our model, we now consider a particulate composite with compressible phases. According to the Hashin-Shtrikman estimate, the LC transforms of the effective

bulk and shear moduli reads

$$\left.\begin{aligned}\frac{1}{\widetilde{k}^*(p)+k_{Hill}(p)}&=\frac{c^{(1)}}{k_{Hill}(p)+k^{(1)^*}(p)}=\frac{c^{(2)}}{k_{Hill}(p)+k^{(2)^*}(p)},\\ \frac{1}{\widetilde{\mu}^*(p)+\mu_{Hill}(p)}&=\frac{c^{(1)}}{\mu_{Hill}(p)+\mu^{(1)^*}(p)}=\frac{c^{(2)}}{\mu_{Hill}(p)+\mu^{(2)^*}(p)}\end{aligned}\right\} \tag{80}$$

with $c^{(i)}$ the volume fraction of phase (i). k_{Hill} and μ_{Hill} are the bulk and shear moduli of Hill's interaction tensor which are functions of the bulk and shear moduli of the matrix (phase 1). The estimates (80) are specified to the case of elastic inclusions in a matrix which is elastic in dilatation and viscoelastic (Maxwellian) in shear. Consequently, the phase moduli read

$$k^{(1)^*}(p)=k_e^{(1)},\quad k^{(2)^*}(p)=k_e^{(2)},\quad \mu^{(1)^*}(p)=\mu_e^{(1)}\frac{p}{p+\frac{1}{\tau^{(1)}}},\quad \mu^{(2)^*}(p)=\mu_e^{(2)}. \tag{81}$$

The Hashin-Shtrikman estimate for the bulk modulus simply reads

$$\widetilde{k}^*(p)=\overline{k}_0+\overline{k}_1\frac{p}{p+\dfrac{1}{\overline{\tau}^{(1)}}}, \tag{82}$$

with

$$\left.\begin{aligned}\overline{k}_0&=\frac{k_e^{(1)}\,k_e^{(2)}}{c^{(1)}k_e^{(2)}+c^{(2)}k_e^{(1)}},\\ \overline{k}_1&=\frac{c^{(1)}k_e^{(1)}(\frac{4}{3}\mu_e^{(1)}+k_e^{(2)})+c^{(2)}k_e^{(2)}(\frac{4}{3}\mu_e^{(1)}+k_e^{(1)})}{\frac{4}{3}\mu_e^{(1)}+c^{(1)}k_e^{(2)}+c^{(2)}k_e^{(1)}},\\ \overline{\tau}^{(1)}&=\tau^{(1)}\left(1+\frac{4\mu_e^{(1)}}{3(c^{(1)}k_e^{(2)}+c^{(2)}k_e^{(1)})}\right).\end{aligned}\right\} \tag{83}$$

Therefore, the effective bulk moduli $\widetilde{k}(t)$ is the sum of a constant (elastic) term and a decreasing exponential (*i.e.* its relaxation spectrum contains a single Dirac mass). In this particular case, the estimate obtained with the model (approximation $(67)_1$ with $M=2$) coincides with the exact result (82). The model yields the exact effective bulk relaxation function for microstructures attaining the Hashin-Shtrikman bound in elasticity. A similar result for the effective shear modulus of incompressible particulate composites has been obtained by Suquet (2012). However, when the phases are compressible

the effective shear modulus $\widetilde{\mu}(t)$ is the sum of three decreasing exponentials as shown by Ricaud and Masson (2009) for elastically homogeneous composites. Its rather lengthy expression is not given here. By contrast with the situation for the effective bulk relaxation, the model of Subsection 4.2 can only provide an approximation for the effective shear modulus. It has been compared to the exact Hashin-Shtrikman estimate with the following material data taken from Xue et al. (2006)

$$\left.\begin{array}{l} k_e^{(1)} = 1\,\mathrm{MPa},\ \ \mu_e^{(1)} = 0.5\,\mathrm{MPa},\ \ \tau^{(1)} = 0.01\,\mathrm{s}, \\ k_e^{(2)} = 50\,\mathrm{MPa},\ \ \mu_e^{(2)} = 18.8\,\mathrm{MPa},\ \ c^{(2)} = 0.2. \end{array}\right\} \tag{84}$$

It can be observed in Figure 6 that the approximation and the exact estimate are indistinguishable.

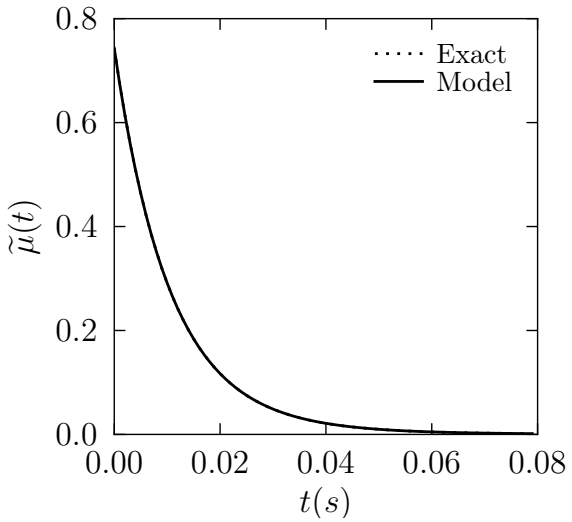

Figure 6: Hashin-Shtrikman estimates of the effective shear relaxation function of compressible particulate composites. The volume fraction of the particles is $c^{(2)} = 0.2$.

5.4. Checkerboard polycrystals

A checkerboard polycrystal is made of the repetition of two crystals rotated by 90°. The constitutive behavior of each single crystal is characterized

by two shear relaxation moduli whose LC transform read

$$\mu^{(k)*}(p) = \mu_e^{(k)} \frac{p}{p + \dfrac{1}{\tau^{(k)}}},\ k = 1,\ 2. \tag{85}$$

$\mu_e^{(k)}$ and $\tau^{(k)}$ are the elastic shear moduli and the characteristic relaxation times of the single crystal. The checkerboard is subjected to anti-plane shear. This problem, analogous to the two-dimensional conductivity problem, has an *exact* solution for the effective shear relaxation modulus (Dykhne, 1970)

$$\widetilde{\mu}^*(p) = \widetilde{\mu}_e \frac{p}{\sqrt{\left(p + \dfrac{1}{\tau^{(1)}}\right)\left(p + \dfrac{1}{\tau^{(2)}}\right)}} \quad \text{with} \quad \widetilde{\mu}_e = \sqrt{\mu_e^{(1)}\,\mu_e^{(2)}}, \tag{86}$$

The viscoelastic response of the checkerboard polycrystal exhibits a continuous effective relaxation spectrum (Masson et al., 2012) and has been investigated under various loading conditions including creep, relaxation and deformation at constant strain-rate in previous studies (Vu et al., 2012; Suquet, 2012; Masson et al., 2012). Here, the harmonic steady-state response of the polycrystal subjected to a sinusoidal macroscopic strain loading with amplitude $\overline{\boldsymbol{\varepsilon}}^*$ and frequency ω: $\overline{\boldsymbol{\varepsilon}}(t) = \overline{\boldsymbol{\varepsilon}}^*\,\mathrm{e}^{\imath\omega t}$ is considered. The *exact* effective storage and loss shear moduli ($\widetilde{\mu}'(\omega)$ and $\widetilde{\mu}''(\omega)$) are classically obtained by using the change of variable $p = \imath\,\omega$ in the expression (86) (Hashin, 1970). They read

$$\widetilde{\mu}'(\omega), \widetilde{\mu}''(\omega) = \frac{\widetilde{\mu}_e\,\omega}{\eta} \sqrt{\frac{1}{2}\left[\eta \mp \left(\frac{1}{\tau^{(1)}\,\tau^{(2)}} - \omega^2\right)\right]} \tag{87}$$

with

$$\eta = \sqrt{\left(\frac{1}{\tau^{(1)}\,\tau^{(2)}} - \omega^2\right)^2 + \omega^2\left(\frac{1}{\tau^{(1)}} + \frac{1}{\tau^{(2)}}\right)^2}. \tag{88}$$

Our approximate model for the real and imaginary parts of the effective complex shear modulus $\widetilde{\mu}^*(\imath\,\omega)$ corresponds to relations (61) with $M = 2$. The coefficients and relaxation times of this approximation have been given by Suquet (2012) to which the reader is referred for detailed expressions. The model is compared with the exact results (87) for the two sets of constitutive data, (78) and (79), corresponding to moderate and high contrasts on the

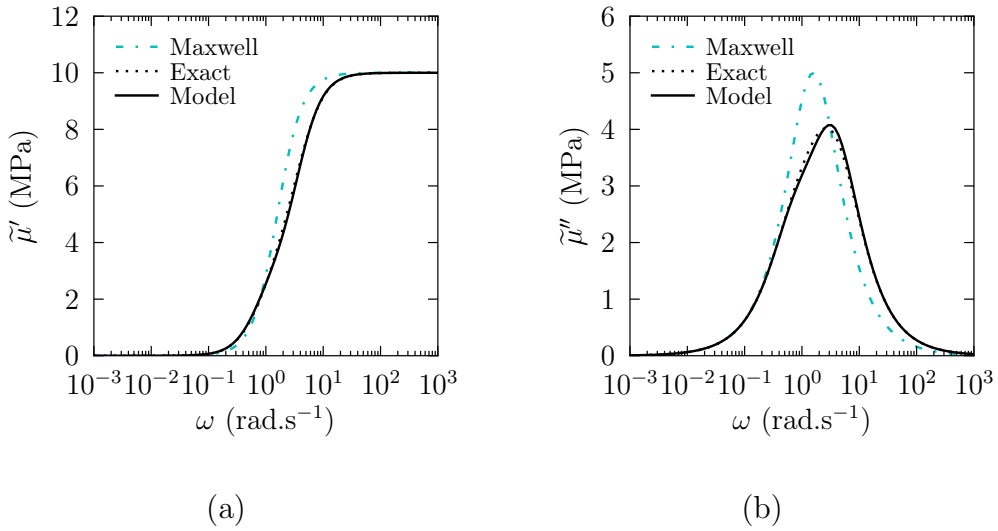

Figure 7: Effective storage (a) and loss (b) shear moduli of a checkerboard polycrystal with moderate contrast on the single crystal relaxation times.

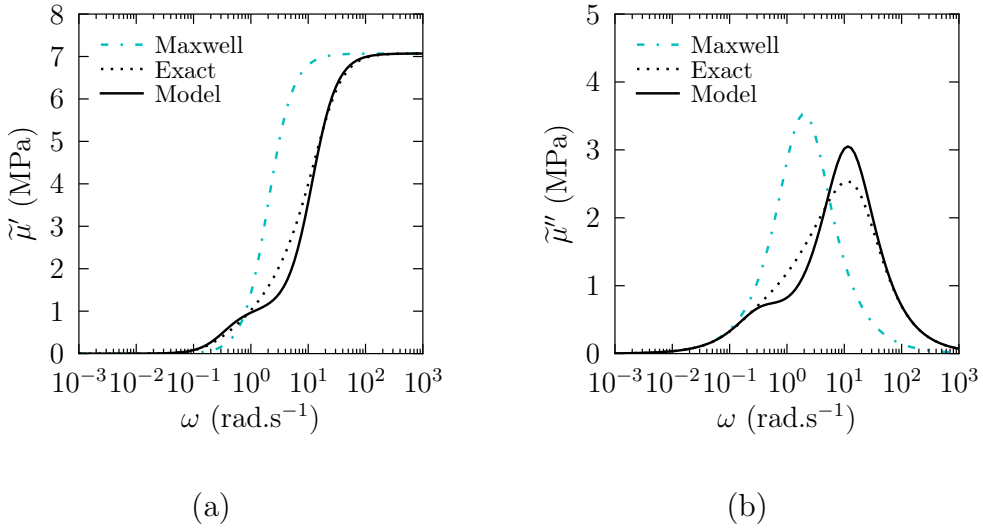

Figure 8: Effective storage (a) and loss (b) shear moduli of a checkerboard polycrystal with high contrast in the single crystal relaxation times.

relaxation times of the crystal. For a moderate contrast (Figure 7), the approximate model yields very accurate estimates for both moduli. When the contrast increases (Figure 8), the agreement is not quite as good, as expected. However, a significant improvement on the Mawellian approximation is observed. In particular, our model delivers a reasonable estimate of the position of the peak of the loss modulus whereas the Maxwell model predicts a shift in the peak towards low frequencies.

5.5. Three-dimensional polycrystals

The model of Subsection 4.2 is now applied to three-dimensional polycrystalline materials with overall isotropy, *i.e.* the grains are equiaxed and all crystalline orientations have equal probability. Each family of grains with a given orientation is a different phase and the heterogeneity between the phases arises from the different crystalline orientations of the grains. The effective response of the polycrystal is estimated by means of the self-consistent scheme.

The anisotropy (elastic and viscous) of the single crystal can be quite general and the linear viscous compliance tensor can be specified either through the entries of a viscous matrix as in Turner and Tomé (1993) for irradiation creep, or described by means of slip systems and slip viscosities. In the latter case, let K denote the number of slip systems and $\boldsymbol{R}^{(k)}$ the Schmid tensor of slip system (k), the linear viscous compliance reads

$$\boldsymbol{M}_v = \sum_k a^k \boldsymbol{R}^{(k)} \otimes \boldsymbol{R}^{(k)}.$$

In most cases the elastic stiffness and viscous compliance of the single crystal belong to the same class of anisotropy (dictated by the symmetries at the single crystal level) and can be decomposed on the same elementary 4th-order tensors $\boldsymbol{R}^{(k)} \otimes \boldsymbol{R}^{(k)}$ (at least for incompressible crystals). The second moments of the elastic or viscous stress fields entering the relations (65) could be expressed by combining the second moments of the resolved shear stress on the different slip systems in the spirit of Liu and Ponte Castañeda (2004). This is not the approach followed here. In the subsequent examples, these second moments have been computed by means of the relations (23) and (24).

5.5.1. Incompressible cubic polycrystals

The elastic or viscous compliance tensor of incompressible single crystals with cubic symmetry reads

$$\boldsymbol{M}^{(r)} = M^a \boldsymbol{K}_a^{(r)} + M^b \boldsymbol{K}_b^{(r)}, \quad M^a = \frac{1}{2\mu^a}, \quad M^b = \frac{1}{2\mu^b}, \tag{89}$$

with μ^a and μ^b the two shear moduli of the cubic single crystal. The projectors $\boldsymbol{K}_a^{(r)}$ and $\boldsymbol{K}_b^{(r)}$ are deduced, after rotation, from the deviatoric projectors $\boldsymbol{K}_a$ and $\boldsymbol{K}_b$ with cubic symmetry:

$$\left.\begin{array}{ll} \boldsymbol{K}_a = \boldsymbol{N} - \boldsymbol{J}, & \boldsymbol{K}_b = \boldsymbol{K} - \boldsymbol{K}_a, \\ \boldsymbol{J} = \dfrac{1}{3}\, \boldsymbol{i} \otimes \boldsymbol{i}, & \boldsymbol{K} = \boldsymbol{I} - \boldsymbol{J}, \end{array}\right\} \tag{90}$$

where $\boldsymbol{N}$ is the fourth-order tensor with cubic symmetry defined as $\boldsymbol{N} = \sum_{i=1}^{3} \boldsymbol{e}_i \otimes \boldsymbol{e}_i \otimes \boldsymbol{e}_i \otimes \boldsymbol{e}_i$ with $(\boldsymbol{e}_1,\, \boldsymbol{e}_2,\, \boldsymbol{e}_3)$ the orthonormal basis associated with the cubic symmetry. As a consequence, the second moment of the stress field for phase (r) reads

$$\boldsymbol{K}_p^{(r)} :: \langle \boldsymbol{s} \otimes \boldsymbol{s} \rangle^{(r)} = \frac{1}{c^{(r)}} \frac{\partial \widetilde{M}}{\partial M^p}\, \overline{\boldsymbol{s}} : \overline{\boldsymbol{s}} \quad \text{with} \quad p = a,\, b. \tag{91}$$

Applying this relation to the elastic and viscous stress fields, one gets

$$\langle \boldsymbol{s}_e : \boldsymbol{M}_v : \boldsymbol{s}_e \rangle = \sum_p M_v^p \frac{\partial \widetilde{M}_e}{\partial M_e^p}\, \overline{\boldsymbol{s}} : \overline{\boldsymbol{s}} \quad \text{with} \quad p = a,\, b \tag{92}$$

and

$$\langle \boldsymbol{s}_v : \boldsymbol{M}_e : \boldsymbol{s}_v \rangle = \sum_p M_e^p \frac{\partial \widetilde{M}_v}{\partial M_v^p}\, \overline{\boldsymbol{s}} : \overline{\boldsymbol{s}} \quad \text{with} \quad p = a,\, b, \tag{93}$$

which leads to the parameters $\overline{M}_1$ and $\overline{\theta}_1$ by means of (68)

$$\overline{M}_1 = \sum_p M_e^p \frac{\partial \widetilde{M}_v}{\partial M_v^p} - \widetilde{M}_e \quad \text{and} \quad \frac{\overline{M}_1}{\overline{\theta}_1} = \sum_p M_v^p \frac{\partial \widetilde{M}_e}{\partial M_e^p} - \widetilde{M}_v \tag{94}$$

where the superscript (d) has been omitted for brevity. The effective shear

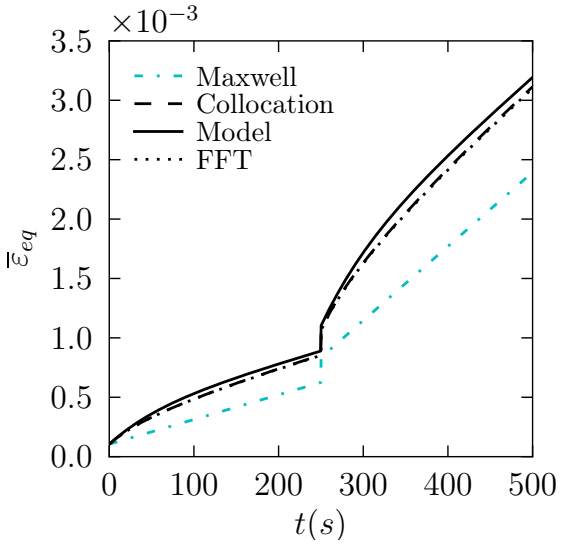

Figure 9: Polycrystals with cubic symmetry. Comparison between the approximate model of Subsection 4.2 (with the self-consistent scheme) and FFT full-field simulations.

modulus $\widetilde{\mu}$ of incompressible isotropic polycrystals made from cubic single crystals is accurately predicted by the self-consistent scheme (Kröner, 1958)

$$3\,\widetilde{\mu}^2 - \mu^b\widetilde{\mu} - 2\mu^a\mu^b = 0. \tag{95}$$

The partial derivatives in (94) are obtained in closed form. The predictions of the resulting (approximate) linear viscoelastic self-consistent scheme are compared with FFT full-field simulations performed on 3D unit-cells containing 4096 grains obtained by Voronoi tessellation. The FFT results have been averaged over 10 different realizations of the unit-cell. The following crystal data have been used

$$\left.\begin{array}{ll} \mu_e^a = 3424 \text{ MPa}, & \mu_e^b = 3014 \text{ MPa} \\ \mu_v^a = 1238 \text{ GPa.s}, & \mu_v^b = 29.3 \text{ GPa.s} \end{array}\right\} \tag{96}$$

The polycrystal is subjected to the stress loading (77) with $t_1 = 250\,\text{s}$. Figure 9 shows a good agreement between the model and full-field results, both in the transient and asymptotic regimes. It is also observed that the collocation method with 5 terms is in close agreement with the FFT results.

5.5.2. Incompressible hexagonal polycrystals

The elastic or viscous compliance tensor of incompressible single crystal with hexagonal symmetry reads

$$\left.\begin{aligned} &\boldsymbol{M}^{(r)} = M^E\,\boldsymbol{K}_E^{(r)} + M^t\,\boldsymbol{K}_t^{(r)} + M^l\,\boldsymbol{K}_l^{(r)},\\ &M^E = \frac{3}{2E^l},\ M^t = \frac{1}{2\mu^t},\ M^l = \frac{1}{2\mu^l}, \end{aligned}\right\} \tag{97}$$

with E^l the longitudinal Young modulus, μ^t the transverse shear modulus and μ^l the longitudinal shear modulus of the hexagonal single crystal. The projectors $\boldsymbol{K}_E^{(r)}$, $\boldsymbol{K}_t^{(r)}$ and $\boldsymbol{K}_l^{(r)}$ are deduced, after rotation, from the transversely isotropic deviatoric projectors $\boldsymbol{K}_E$, $\boldsymbol{K}_t$ and $\boldsymbol{K}_l$ defined as

$$\left.\begin{aligned} &\boldsymbol{K}_E = \frac{1}{6}(\boldsymbol{i} - 3\,\boldsymbol{c}\otimes\boldsymbol{c})\otimes(\boldsymbol{i} - 3\,\boldsymbol{c}\otimes\boldsymbol{c}),\\ &\boldsymbol{K}_l = 2\left([\boldsymbol{c}\otimes\boldsymbol{I}\otimes\boldsymbol{c}]^{(s)} - \boldsymbol{c}\otimes\boldsymbol{c}\otimes\boldsymbol{c}\otimes\boldsymbol{c}\right),\\ &\boldsymbol{K}_t = \boldsymbol{K} - \boldsymbol{K}_E - \boldsymbol{K}_l, \quad \boldsymbol{K} = \boldsymbol{I} - \boldsymbol{J}, \end{aligned}\right\} \tag{98}$$

where $\boldsymbol{c}$ is the senary axis of the hexagonal crystalline structure. The relations (91) to (94) used for crystals with cubic symmetry apply equally to hexagonal crystals by extending the summation to $p = E,\, t,\, l$. When the general equations of the self-consistent scheme for hexagonal materials (see for instance Berryman, 2005) are particularized to incompressible phases, the self-consistent estimate for the macroscopic shear modulus of isotropic hexagonal polycrystals is solution of the cubic equation

$$\widetilde{\mu}^3 + \frac{1}{9}E^l\widetilde{\mu}^2 - \frac{2}{27}\left[E^l(\mu^t + \mu^l) + 6\mu^t\mu^l\right]\widetilde{\mu} - \frac{4}{27}E^l\mu^t\mu^l = 0. \tag{99}$$

Analytical expressions for the second moments defining the approximate model (94) can be derived in closed form from (99). The predictions of the model are compared in Figure 10 with FFT full-field simulations. The polycrystal is subjected to the stress loading (77) with $t_1 = 250\,\mathrm{s}$ and the single crystal data are:

$$\left.\begin{aligned} &E_e^l = 11846\ \text{MPa}, \quad \mu_e^t = 3424\ \text{MPa}, \quad \mu_e^l = 3424\ \text{MPa}\\ &E_v^l = 3249\ \text{GPa.s}, \quad \mu_v^t = 929\ \text{GPa.s}, \quad \mu_v^l = 14.63\ \text{GPa.s} \end{aligned}\right\} \tag{100}$$

This dataset is representative of ice single crystals which are characterized by an almost isotropic elastic behaviour and a strong viscous anisotropy. The

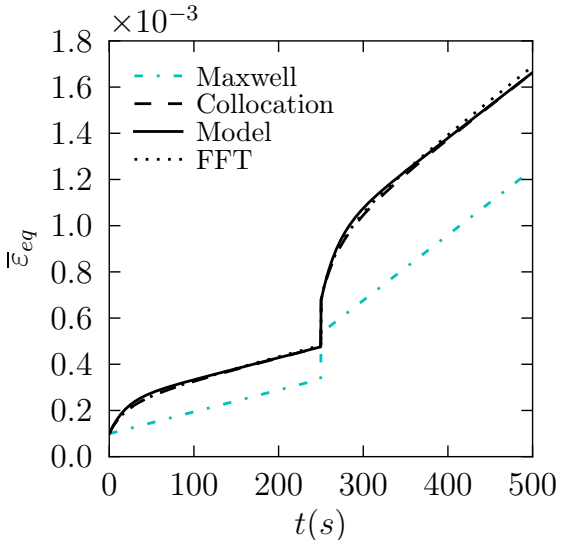

Figure 10: Isotropic polycrystals composed of single crystals with hexagonal symmetry. Comparison between the approximate model of Subsection 4.2 (with the self-consistent scheme) and FFT full-field simulations.

contrast between the relaxation times of the single crystal in the different directions is of the order of 60. Once again the predictions of the model are observed to be in close agreement with the reference FFT results. In particular the significant decrease of the creep strain-rate during the transient regime, due to the (almost) elastic isotropy and to the strong viscous anisotropy of the single crystal, is correctly captured by the model (unlike the Maxwellian approximation).

6. Concluding remarks

In this study two new asymptotic relations for the effective creep function of linear viscoelastic composites have been derived and their physical interpretation at short and large times has been clarified, improving on a previous and similar investigation on relaxation functions (Suquet, 2012). These exact relations involve second-order moments per phase of the solutions of the purely elastic and purely viscous problems. These asymptotic relations have been applied to harmonic loadings. In this context, they provide a set of asymptotic relations in the frequency domain on the storage and loss mod-

uli of the composite. Although these conditions have been formulated for mixtures of Maxwellian constituents (irradiation creep of metallic or ceramic polycrystals, for instance), it is worth noting that similar relations hold for more general viscoelastic behaviors of the constituents.

Based on these relations, an approximate model has been proposed for the creep function of linear viscoelastic heterogeneous materials. This model approximates the retardation spectrum of the composite by a single discrete Dirac mass. The retardation time and its corresponding weight depend again on the coupling between the elastic (resp. viscous) local compliances and the viscous (resp. elastic) stress field fluctuations. This model has been applied to predict the effective creep, relaxation and harmonic responses of different composites and polycrystals. Its accuracy has been assessed by comparison with exact analytical results, reference full-field simulations and collocation results. A very good agreement is obtained when the contrast on the phase relaxation times remains moderate.

Acknowledgements

This study was partly funded by the French 'Agence Nationale de la Recherche' (project ELVIS, #ANR-08-BLAN-0138). The authors are grateful to H. Moulinec (LMA-CNRS, France) for providing the FFT simulations shown in figures 4, 9 and 10.

References

Berryman, J., 2005. Bounds and self-consistent estimates for elastic constants of random polycrystals with hexagonal, trigonal, and tetragonal symmetries. J. Mech. Phys. Solids **53**, 2141–2173.

Beurthey, S., Zaoui, A., 2000. Structural morphology and relaxation spectra of viscoelastic heterogeneous materials. Eur. J. Mech. A/Solids **19**, 1–16.

Bobeth, M., Diener, G., 1987. Static and thermoelastic field fluctuations in multiphase composites. J. Mech. Phys. Solids **35**, 137–149.

Bradshaw, R., Brinson, L., 1997. A sign control method for fitting and interconverting material functions for linearly viscoelastic solids. Mech. Time-Depend. Mater. **1**, 85–108.

Brenner, R., Masson, R., 2005. Improved affine estimates for nonlinear viscoelastic composites. Eur. J. Mech. A/Solids **24**, 1002–1015.

Brenner, R., Masson, R., Castelnau, O., Zaoui, A., 2002. A "quasi-elastic" affine formulation for the homogenized behaviour of nonlinear viscoelastic polycrystals and composites. Eur. J. Mech. A/Solids **21**, 943–960.

Christensen, R., 1971. Theory of Viscoelasticity: An introduction. Academic Press, New York.

Christensen, R., Lo, K., 1979. Solutions for effective shear properties in three phase sphere and cylinder models. J. Mech. Phys. Solids **27**, 315–330.

Cost, T., Becker, E., 1970. A multidata method of approximate laplace transform inversion. Int. J. Num. Meth. Engng **2**, 207–219.

Dykhne, A. M., 1970. Conductivity of a two-dimensional two-phase system. Soviet Physics JETP **32**, 63–65.

Eyre, D., Milton, G., Lakes, R., 2002. Bounds for interpolating complex effective moduli of viscoelastic materials from measured data. Rheol. Acta **41**, 461–470.

Francfort, G., Leguillon, D., Suquet, P., 1983. Homogénéisation de milieux visco-élastiques de Kelvin-Voigt. C.R. Acad. Sci., Ser. I **296**, 287–290.

Hashin, Z., 1965. Viscoelastic behavior of heterogeneous media. J. Appl. Mech. **32**, 630–636.

Hashin, Z., 1970. Complex moduli of viscoelastic composites – I. General theory and application to particulate composites. Int. J. Solids Struct. **6**, 539–552.

Hervé, E., Zaoui, A., 1990. Modelling the effective behavior of nonlinear matrix-inclusion composites. Eur. J. Mech. A/ Solids **9**, 505–515.

Idiart, M., Moulinec, H., Ponte Castañeda, P., Suquet, P., 2006. Macroscopic behavior and field fluctuations in viscoplastic composites: second-order estimates versus full-field simulations. J. Mech. Phys. Solids **54**, 1029–1063.

Kowalczyk-Gajewska, K., Petryk, H., 2011. Sequential linearization method for viscous/elastic heterogeneous materials. Eur. J. Mech. A/Solids **30**, 650–664.

Kreher, W., 1990. Residual stresses and stored elastic energy of composites and polycrystals. J. Mech. Phys. Solids **38**, 115–128.

Kröner, E., 1958. Berechnung der elastichen Konstanten des Vielkristalls aus den Konstanten des Einkristalls. Z. Phys. **151**, 504–518.

Labé, A., Moulinec, H., Suquet, P., 2011. CraFT: Composite response and Fourier Transforms. Tech. Rep., CNRS/LMA, `http://craft.lma.cnrs-mrs.fr/`.

Lahellec, N., Suquet, P., 2007. Effective behavior of linear vicoelastic composites: a time-integration approach. Int. J. Solids Struct. **44**, 507–529.

Laws, N., Mc Laughlin, R., 1978. Self-consistent estimates for the viscoelastic creep compliance of composite materials. Proc. R. Soc. London A **359**, 251–273.

Lebensohn, R., 2001. N-site modelling of a 3D viscoplastic polycrystal using Fast Fourier Transforms. Acta Mater. **49**, 2723–2737.

Lebensohn, R., Kanjarla, A., Eisenlohr, P., 2012. An elasto-viscoplastic formulation based on fast Fourier transforms for the prediction of micromechanical fields in polycrystalline materials. Int. J. Plast. **32-33**, 59–69.

Lebensohn, R., Rollett, A., Suquet, P., 2011. Fast Fourier transform-based modelling for the determination of micromechanical fields in polycrystals. JOM **63** (3), 13–18.

Liu Y., Ponte Castañeda P., 2004. Second-order theory for the effective behavior and field fluctuations in viscoplastic polycrystals, J. Mech. Phys. Solids **52**, 467–495.

Mandel, J., 1966. Cours de Mécanique des Milieux Continus. Gauthier-Villars, Paris.

Masson, R., Brenner, R., Castelnau, O., 2012. Incremental homogenization approach for ageing viscoelastic polycrystals. C.R. Mécanique **340**, 378–386.

Masson, R., Zaoui, A., 1999. Self-consistent estimates for the rate-dependent elastoplastic behaviour of polycrystalline materials. J. Mech. Phys. Solids **47**, 1543–1568.

Moulinec, H., Suquet, P., 1998. A numerical method for computing the overall response of nonlinear composites with complex microstructure. Comp. Meth. Appl. Mech. Engng **157**, 69–94.

Ponte Castañeda, P., Suquet, P., 1998. Nonlinear composites. Adv. Appl. Mech. **34**, 171–302.

Rekik, A., Brenner, R., 2011. Optimization of the collocation inversion method for the linear viscoelastic homogenization. Mech. Res. Comm. **38**, 305–308.

Ricaud, J.-M., Masson, R., 2009. Effective properties of linear viscoelastic heterogeneous media: Internal variables formulation and extension to ageing behaviours. Int. J. Solids Struct. **46**, 1599–1606.

Rougier, Y., Stolz, C., Zaoui, A., 1993. Représentation spectrale en viscoélasticité linéaire des matériaux hétérogènes. C.R. Acad. Sci., Ser. II **316**, 1517–1522.

Sanchez-Hubert, J., Sanchez-Palencia, E., 1978. Sur certains problèmes physiques d'homogénéisation donnant lieu à des phénomènes de relaxation. C.R. Acad. Sci., Ser. A **286**, 903–906.

Schapery, R., 1962. Approximate methods of transform inversion for viscoelastic stress analysis. In: Proc. U.S. Nat. Congr. Appl. Mech. ASME 4th. ASME, New-York, pp. 1075–1085.

Schapery, R., 1974. Viscoelastic behavior and analysis of composite materials. In: Sendeckyj, G. (Ed.), Mechanics of Composite Materials. Academic Press, New-York, pp. 85–167.

Suquet, P., 1987. Elements of Homogenization for Inelastic Solid Mechanics. In: Sanchez-Palencia, E., Zaoui, A. (Eds.), Homogenization Techniques for Composite Media. Vol. **272** of Lecture Notes in Physics. Springer Verlag, New York, pp. 193–278.

Suquet, P., 1995. Overall properties of nonlinear composites : a modified secant moduli theory and its link with Ponte Castañeda's nonlinear variational procedure. C.R. Acad. Sci., Ser. IIb **320**, 563–571.

Suquet, P., 2012. Four exact relations for the effective relaxation function of linear viscoelastic composites. C.R. Mécanique **340**, 387–399.

Suquet, P., Moulinec, H., 1997. Numerical simulation of the effective properties of a class of cell materials. In: Golden, K., Grimmett, G., James, R., Milton, G., Sen, P. (Eds.), Mathematics of multiscale materials. Vol. **99** of IMA Lecture Notes. Springer-Verlag, New-York, pp. 277–287.

Suquet, P., Moulinec, H., Castelnau, O., Lahellec, N., Grennerat, F., Duval, P., Brenner, R., 2012. Multi-scale modeling of the mechanical behavior of polycrystalline ice under transient creep. Procedia IUTAM **3**, 76–90.

Tschoegl, N., 1989. The phenomenological theory of linear viscoelastic behavior. An introduction. Springer-Verlag, Berlin.

Turner, P., Tomé, C., 1993. Self-consistent modeling of visco-elastic polycrystals: application to irradiation creep and growth. J. Mech. Phys. Solids **41**, 1191–1211.

Vu, Q. H., Brenner, R., Castelnau, O., Moulinec, H., Suquet, P., 2012. A self-consistent estimate for linear viscoelastic polycrystals with internal variables inferred from the collocation method. Modell. Simul. Mater. Sci. Eng. **20**, 024003.

Xue, L., Borodin, O., Smith, G. D., Nairn, J., 2006. Micromechanics simulations of the viscoelastic properties of highly filled composites by the material point method (MPM). Modell. Simul. Mater. Sci. Eng. **14**, 703–720.

Appendix A. Stieljes convolution and Laplace-Carson transform

The Stieljes convolution product ($\star$) of two functions f and g is the derivative of their usual convolution product. When g is a differentiable function of time the Stieljes product $f \star g$ reads

$$(f \star g)(t) = \frac{\mathrm{d}}{\mathrm{d}t}(f * g)(t) = \int_0^t f(t-u)\,\dot{g}(u)\,\mathrm{d}u \tag{A.1}$$

When g is only piecewise continuous and differentiable, its time derivative in (A.1) contains Dirac masses at discontinuity points t_n and the Stieljes convolution product (A.1) must be understood as

$$(f \star g)(t) = \int_0^t f(t-u)\,\dot{g}(u)\,\mathrm{d}u + \sum_n f(t-t_n)\,[g]_n \tag{A.2}$$

where $[g]_n$ is the discontinuity of g at time t_n and $\dot{g}(u)$ is the usual derivative of g at all u's where it is differentiable.

The Laplace-Carson transform of a function $f(t)$ is defined by

$$f^*(p) = p \int_0^{+\infty} e^{-pt}\, f(t)\,\mathrm{d}t. \tag{A.3}$$

From (A.2) and (A.3), it follows that

$$(f \star g)^*(p) = f^*(p)\, g^*(p). \tag{A.4}$$

It is also useful to note that the Laplace-Carson transform of the time derivative function $\dot{f}(t)$ reads

$$\dot{f}^*(p) = p(f^*(p) - f(0)). \tag{A.5}$$

The initial and final value theorems, linking the function $f(t)$ and its Laplace-Carson transform $f^*(p)$ at short and large times, read

$$\lim_{t\to 0^+} f(t) = \lim_{p\to+\infty} f^*(p) \quad \text{and} \quad \lim_{t\to+\infty} f(t) = \lim_{p\to 0} f^*(p). \tag{A.6}$$

By making use of (A.5), it is also noted that

$$\lim_{t\to+\infty} \dot{f}(t) = \lim_{p\to 0} p f^*(p). \tag{A.7}$$

Appendix B. Proof of relations (20) and (21)

Proof of (20). Multiply the constitutive relation (5) by the elastic stress field $\boldsymbol{\sigma}_e(\boldsymbol{x})$, average over V and take the limit of both sides of the equation as t tends to 0^+:

$$\lim_{t\to 0^+} \langle \boldsymbol{\sigma}_e : \dot{\boldsymbol{\varepsilon}} \rangle (t) = \lim_{t\to 0^+} \left[\langle \boldsymbol{\sigma}_e : \boldsymbol{M}_e : \dot{\boldsymbol{\sigma}} \rangle (t) + \langle \boldsymbol{\sigma}_e : \boldsymbol{M}_v : \boldsymbol{\sigma} \rangle (t) \right]. \tag{B.1}$$

Hill's lemma can be applied to both sides of this relation, recalling, for the right-hand side that $\boldsymbol{M}_e : \boldsymbol{\sigma}_e = \boldsymbol{\varepsilon}_e$ is a compatible strain field:

$$\lim_{t\to 0^+} \overline{\boldsymbol{\sigma}}_e : \dot{\overline{\boldsymbol{\varepsilon}}}(t) = \lim_{t\to 0^+} \left[\ \overline{\boldsymbol{\varepsilon}}_e : \dot{\overline{\boldsymbol{\sigma}}}(t) + \langle \boldsymbol{\sigma}_e : \boldsymbol{M}_v : \boldsymbol{\sigma} \rangle (t) \ \right]. \tag{B.2}$$

Since $\overline{\boldsymbol{\sigma}}$ does not depend on t (creep loading), one has:

$$\overline{\boldsymbol{\sigma}}_e = \overline{\boldsymbol{\sigma}} \quad \text{and} \quad \dot{\overline{\boldsymbol{\sigma}}}(t) = 0, \quad \forall t \in]0, +\infty[. \tag{B.3}$$

Using (12), relation (B.2) gives

$$\overline{\boldsymbol{\sigma}} : \dot{\overline{\boldsymbol{\varepsilon}}}(0^+) = \langle \boldsymbol{\sigma}_e : \boldsymbol{M}_v : \boldsymbol{\sigma}_e \rangle \quad \text{with} \quad \dot{\overline{\boldsymbol{\varepsilon}}}(0^+) = \lim_{t\to 0^+} \dot{\overline{\boldsymbol{\varepsilon}}}(t). \tag{B.4}$$

Proof of (21). Multiplying the constitutive relation (5) by the stress field $\boldsymbol{\sigma}(\boldsymbol{x}, t)$ and averaging over V, one gets:

$$\overline{\boldsymbol{\sigma}} : \dot{\overline{\boldsymbol{\varepsilon}}}(s) = \langle \boldsymbol{\sigma} : \boldsymbol{M}_e : \dot{\boldsymbol{\sigma}} \rangle (s) + \langle \boldsymbol{\sigma} : \boldsymbol{M}_v : \boldsymbol{\sigma} \rangle (s),$$

(on the left-hand side, use has been made of Hill's lemma and of the loading condition $\langle \boldsymbol{\sigma}(s) \rangle = \overline{\boldsymbol{\sigma}}$). Integration in time gives:

$$\overline{\boldsymbol{\sigma}} : \left(\overline{\boldsymbol{\varepsilon}}(t) - \overline{\boldsymbol{\varepsilon}}(0^+) \right) = \frac{1}{2} \left[\langle \boldsymbol{\sigma}(s) : \boldsymbol{M}_e : \boldsymbol{\sigma}(s) \rangle \right]_{s=0}^{s=t} + \int_0^t \langle \boldsymbol{\sigma}(s) : \boldsymbol{M}_v : \boldsymbol{\sigma}(s) \rangle \ \mathrm{d}s. \tag{B.5}$$

The left-hand side of the equation (B.5) is the energy supplied by the external device to apply a constant overall stress from $s = 0$ to $s = t$. The first term in the right-hand side of (B.5) is the elastic energy stored in the composite between 0 and t which can be re-written as:

$$\frac{1}{2} \langle \boldsymbol{\sigma}(t) : \boldsymbol{M}_e : \boldsymbol{\sigma}(t) \rangle - \frac{1}{2} \langle \boldsymbol{\sigma}_e : \boldsymbol{M}_e : \boldsymbol{\sigma}_e \rangle .$$

Note that the stored energy is always positive according to the variational property of $\boldsymbol{\sigma}_e$:

$$\langle \boldsymbol{\sigma}_e : \boldsymbol{M}_e : \boldsymbol{\sigma}_e \rangle = \inf_{\boldsymbol{\tau} \in \mathcal{S}(\overline{\boldsymbol{\sigma}})} \langle \boldsymbol{\tau} : \boldsymbol{M}_e : \boldsymbol{\tau} \rangle \leq \langle \boldsymbol{\sigma}(t) : \boldsymbol{M}_e : \boldsymbol{\sigma}(t) \rangle \,. \tag{B.6}$$

where

$$\mathcal{S}(\overline{\boldsymbol{\sigma}}) = \{ \boldsymbol{\tau}, \quad \text{div } \boldsymbol{\tau} = \boldsymbol{0}, \quad \langle \boldsymbol{\tau} \rangle = \overline{\boldsymbol{\sigma}}. \} \,. \tag{B.7}$$

The stored energy remains finite as $t \to +\infty$ and tends to

$$\frac{1}{2} \langle \boldsymbol{\sigma}_v : \boldsymbol{M}_e : \boldsymbol{\sigma}_v \rangle - \langle \boldsymbol{\sigma}_e : \boldsymbol{M}_e : \boldsymbol{\sigma}_e \rangle = \frac{1}{2} \langle \boldsymbol{\sigma}_v : \boldsymbol{M}_e : \boldsymbol{\sigma}_v \rangle - \frac{1}{2} \overline{\boldsymbol{\sigma}} : \overline{\boldsymbol{\varepsilon}}(0^+). \tag{B.8}$$

The second term in the right-hand side of (B.5) is the energy dissipated in the creep test between $s = 0$ and $s = t$ and is unbounded in the limit as $t \to +\infty$. It can be compared to the energy dissipated by the Maxwellian approximation of $\widetilde{\boldsymbol{M}}(t)$:

$$\begin{aligned} \int_0^t \langle \boldsymbol{\sigma}(s) : \boldsymbol{M}_v : \boldsymbol{\sigma}(s) \rangle \, \mathrm{d}s = & \\ \int_0^t \langle \boldsymbol{\sigma}_v : \boldsymbol{M}_v : \boldsymbol{\sigma}_v \rangle \, \mathrm{d}s + \int_0^t \langle (\boldsymbol{\sigma}(s) - \boldsymbol{\sigma}_v) : \boldsymbol{M}_v : (\boldsymbol{\sigma}(s) - \boldsymbol{\sigma}_v) \rangle \, \mathrm{d}s & \\ = \overline{\boldsymbol{\sigma}} : t\widetilde{\boldsymbol{M}}_v : \overline{\boldsymbol{\sigma}} + \int_0^t \langle (\boldsymbol{\sigma}(s) - \boldsymbol{\sigma}_v) : \boldsymbol{M}_v : (\boldsymbol{\sigma}(s) - \boldsymbol{\sigma}_v) \rangle \, \mathrm{d}s, & \end{aligned}$$

where use has been made of the following consequence of Hill's lemma:

$$\langle (\boldsymbol{\sigma}(s) - \boldsymbol{\sigma}_v) : \boldsymbol{M}_v : \boldsymbol{\sigma}_v \rangle = \langle (\boldsymbol{\sigma}(s) - \boldsymbol{\sigma}_v) : \dot{\boldsymbol{\varepsilon}}_v \rangle = (\overline{\boldsymbol{\sigma}} - \overline{\boldsymbol{\sigma}}) : \dot{\overline{\boldsymbol{\varepsilon}}}_v = 0.$$

Upon multiplication of the constitutive relations in (7) by $\boldsymbol{\sigma} - \boldsymbol{\sigma}_v$ and averaging over V one gets:

$$\langle (\boldsymbol{\sigma} - \boldsymbol{\sigma}_v) : \boldsymbol{M}_v : (\boldsymbol{\sigma} - \boldsymbol{\sigma}_v) \rangle \, (s) = - \langle (\dot{\boldsymbol{\sigma}} - \dot{\boldsymbol{\sigma}}_v) : \boldsymbol{M}_e : (\boldsymbol{\sigma} - \boldsymbol{\sigma}_v) \rangle \, (s).$$

and after integration in time:

$$\begin{aligned} \int_0^t \langle (\boldsymbol{\sigma}(s) - \boldsymbol{\sigma}_v) : \boldsymbol{M}_v : (\boldsymbol{\sigma}(s) - \boldsymbol{\sigma}_v) \rangle \, \mathrm{d}s = & \\ - \frac{1}{2} \Big[\, \langle (\boldsymbol{\sigma}(s) - \boldsymbol{\sigma}_v) : \boldsymbol{M}_e : (\boldsymbol{\sigma}(s) - \boldsymbol{\sigma}_v) \rangle \, \Big]_{s=0}^{s=t}. & \end{aligned}$$

Making use of the asymptotic properties of the stress field we finally obtain in the limit as $t \to +\infty$:

$$\int_0^{+\infty} \langle (\boldsymbol{\sigma}(s) - \boldsymbol{\sigma}_v) : \boldsymbol{M}_v : (\boldsymbol{\sigma}(s) - \boldsymbol{\sigma}_v) \rangle \, \mathrm{d}s = \\ \frac{1}{2} \langle (\boldsymbol{\sigma}_e - \boldsymbol{\sigma}_v) : \boldsymbol{M}_e : (\boldsymbol{\sigma}_e - \boldsymbol{\sigma}_v) \rangle = \frac{1}{2} \langle \boldsymbol{\sigma}_v : \boldsymbol{M}_e : \boldsymbol{\sigma}_v \rangle - \frac{1}{2} \langle \boldsymbol{\sigma}_e : \boldsymbol{M}_e : \boldsymbol{\sigma}_e \rangle . \tag{B.9}$$

Finally, putting together (B.5), (B.8) and (B.9) gives (21).

Appendix C. Proof of relations (37) and (38)

The proofs of these asymptotic relations, for the macroscopic strain history (31), are similar to those of relations (20) and (21). Elements of proofs are given hereafter.

Proof of (37). Thanks to Hill's lemma, relation (B.1) together with the strain loading $\overline{\boldsymbol{\varepsilon}}(t) = \overline{\boldsymbol{\varepsilon}}_0 + t\dot{\overline{\boldsymbol{\varepsilon}}}$ gives

$$\overline{\boldsymbol{\sigma}}_e : \dot{\overline{\boldsymbol{\varepsilon}}} = \lim_{t \to 0^+} \left[\ \overline{\boldsymbol{\varepsilon}}_0 : \dot{\overline{\boldsymbol{\sigma}}}(t) + \langle \boldsymbol{\sigma}_e : \boldsymbol{M}_v : \boldsymbol{\sigma} \rangle \, (t) \ \right] . \tag{C.1}$$

The result (37) follows by using the asymptotic property of the stress field, solution of the local problem (33) as $t \to +\infty$, and noting that $\overline{\boldsymbol{\sigma}}_e = \widetilde{\boldsymbol{L}}_e : \overline{\boldsymbol{\varepsilon}}_0$.

Proof of (38). By multiplying the constitutive relation (5) by the stress field $\boldsymbol{\sigma}(\boldsymbol{x}, t)$ and averaging over V, one gets:

$$\overline{\boldsymbol{\sigma}}(s) : \dot{\overline{\boldsymbol{\varepsilon}}} = \langle \boldsymbol{\sigma} : \boldsymbol{M}_e : \dot{\boldsymbol{\sigma}} \rangle \, (s) + \langle \boldsymbol{\sigma} : \boldsymbol{M}_v : \boldsymbol{\sigma} \rangle \, (s).$$

The term on the left-hand side follows from Hill's lemma and the strain loading history (31). Integration in time gives:

$$\dot{\overline{\boldsymbol{\varepsilon}}} : \int_0^t \overline{\boldsymbol{\sigma}}(s) \, \mathrm{d}s = \frac{1}{2} \left[\langle \boldsymbol{\sigma}(s) : \boldsymbol{M}_e : \boldsymbol{\sigma}(s) \rangle \right]_{s=0}^{s=t} + \int_0^t \langle \boldsymbol{\sigma}(s) : \boldsymbol{M}_v : \boldsymbol{\sigma}(s) \rangle \, \mathrm{d}s. \tag{C.2}$$

In the limit $t \to +\infty$, the stored elastic energy reads

$$\frac{1}{2} \langle \boldsymbol{\sigma}_v : \boldsymbol{M}_e : \boldsymbol{\sigma}_v \rangle - \frac{1}{2} \overline{\boldsymbol{\sigma}}(0^+) : \overline{\boldsymbol{\varepsilon}}_0 \tag{C.3}$$

and the dissipated viscous energy takes the form

$$\dot{\overline{\boldsymbol{\varepsilon}}} : \int_0^{+\infty} (2\,\overline{\boldsymbol{\sigma}}(s) - \overline{\boldsymbol{\sigma}}_v) \, \mathrm{d}s + \int_0^{+\infty} \langle (\boldsymbol{\sigma}(s) - \boldsymbol{\sigma}_v) : \boldsymbol{M}_v : (\boldsymbol{\sigma}(s) - \boldsymbol{\sigma}_v) \rangle \, \mathrm{d}s. \tag{C.4}$$

Besides, using the asymptotic properties of the stress field, the following equality holds:

$$\int_0^{+\infty} \langle (\boldsymbol{\sigma}(s) - \boldsymbol{\sigma}_v) : \boldsymbol{M}_v : (\boldsymbol{\sigma}(s) - \boldsymbol{\sigma}_v) \rangle \, \mathrm{d}s = \frac{1}{2} \langle \boldsymbol{\sigma}_e : \boldsymbol{M}_e : \boldsymbol{\sigma}_e \rangle + \frac{1}{2} \langle \boldsymbol{\sigma}_v : \boldsymbol{M}_e : \boldsymbol{\sigma}_v \rangle - \overline{\boldsymbol{\varepsilon}}_0 : \widetilde{\boldsymbol{L}}_v : \dot{\overline{\boldsymbol{\varepsilon}}}. \quad \text{(C.5)}$$

The result (38) is finally obtained by gathering (C.2) to (C.5).

Appendix D. Proof of the relations (52) and (53)

Proof of (52): Under a prescribed (and constant in time) macroscopic stress $\overline{\boldsymbol{\sigma}}$ the variational property of $\boldsymbol{\sigma}^*(\boldsymbol{x}, p)$ reads as:

$$\begin{aligned} \overline{\boldsymbol{\sigma}}^*(p) : \widetilde{\boldsymbol{M}}^*(p) : \overline{\boldsymbol{\sigma}}^*(p) &= \langle \boldsymbol{\sigma}^*(p) : \boldsymbol{M}^*(p) : \boldsymbol{\sigma}^*(p) \rangle \\ &= \inf_{\boldsymbol{\sigma},\, \langle \boldsymbol{\sigma} \rangle = \overline{\boldsymbol{\sigma}}} \langle \boldsymbol{\sigma} : \boldsymbol{M}^*(p) : \boldsymbol{\sigma} \rangle \,, \ \forall p \in [0, +\infty[, \quad \text{(D.1)} \end{aligned}$$

It follows from a classical lemma on the derivative of a stationary value of an energy (Ponte Castañeda and Suquet, 1998) that, for any parameter q:

$$\overline{\boldsymbol{\sigma}} : \frac{\partial \widetilde{\boldsymbol{M}}^*}{\partial q} : \overline{\boldsymbol{\sigma}} = \left\langle \boldsymbol{\sigma}^*(p) : \frac{\partial \boldsymbol{M}}{\partial q} : \boldsymbol{\sigma}^*(p) \right\rangle . \quad \text{(D.2)}$$

Choosing $q = 1/p$ and using the expression (46) to express the derivative of $\boldsymbol{M}^*(p)$ with respect to $1/p$ in (D.2) yields

$$\overline{\boldsymbol{\sigma}} : \frac{\partial \widetilde{\boldsymbol{M}}^*}{\partial q} : \overline{\boldsymbol{\sigma}} = \langle \boldsymbol{\sigma}^*(p) : \boldsymbol{M}_v : \boldsymbol{\sigma}^*(p) \rangle . \quad \text{(D.3)}$$

The asymptotic result $(12)_1$ for short times read in Laplace space

$$\lim_{p \to +\infty} \boldsymbol{\sigma}^*(\boldsymbol{x}, p) = \boldsymbol{\sigma}_e(\boldsymbol{x}),$$

and passing to the limit in (D.3) as $p \to +\infty$ yields (52). Also, by noting that $(14)_1$ can be written in Laplace space as

$$\lim_{p \to 0} \boldsymbol{\sigma}^*(\boldsymbol{x}, p) = \boldsymbol{\sigma}_v(\boldsymbol{x}),$$

the limit of (D.3) as $p \to 0$ yields the classical result (51).

Proof of (53): The variational property of $\boldsymbol{\sigma}^*(\boldsymbol{x}, p)$ can be alternatively written as:

$$\overline{\boldsymbol{\sigma}}^* : \widetilde{\boldsymbol{\mathcal{M}}}^*(p) : \overline{\boldsymbol{\sigma}}^* = \langle \boldsymbol{\sigma}^*(p) : \boldsymbol{\mathcal{M}}^*(p) : \boldsymbol{\sigma}^*(p) \rangle \\ = \inf_{\boldsymbol{\sigma},\, \langle \boldsymbol{\sigma} \rangle = \overline{\boldsymbol{\sigma}}} \langle \boldsymbol{\sigma} : \boldsymbol{\mathcal{M}}^*(p) : \boldsymbol{\sigma} \rangle \,. \quad \text{(D.4)}$$

It follows from the same lemma and from (47) that

$$\overline{\boldsymbol{\sigma}} : \frac{\partial \widetilde{\boldsymbol{\mathcal{M}}}^*}{\partial p}(p) : \overline{\boldsymbol{\sigma}} = \langle \boldsymbol{\sigma}^*(p) : \boldsymbol{M}_e : \boldsymbol{\sigma}^*(p) \rangle \,. \quad \text{(D.5)}$$

By making use of $(14)_1$ and passing to the limit in (D.5) as $p \to 0$, one gets (53). Similarly, the classical result (50) is retrieved asymptotically with $(12)_1$ and (D.5) as $p \to +\infty$.

Appendix E. Effective constitutive relations and internal variables

As shown by Ricaud and Masson (2009) and Vu et al. (2012) the approximation by Prony series is equivalent to a formulation of the overall constitutive relations by internal variables. When the formulation based on the relaxation function is chosen (primal model), the effective constitutive relations can be written as

$$\overline{\boldsymbol{\sigma}}(t) = \sum_{i=1}^{M} \overline{\boldsymbol{L}}_i : (\overline{\boldsymbol{\varepsilon}}(t) - \boldsymbol{\alpha}_i(t)) \quad \text{(E.1)}$$

with

$$\overline{\tau}_i \dot{\boldsymbol{\alpha}}_i(t) + \boldsymbol{\alpha}_i(t) = \overline{\boldsymbol{\varepsilon}}(t), \quad \boldsymbol{\alpha}_i(0) = \boldsymbol{0}. \quad \text{(E.2)}$$

When the formulation based on the creep function is chosen (dual model), the effective constitutive relations read as

$$\overline{\boldsymbol{\varepsilon}}(t) = \widetilde{\boldsymbol{M}}_0 : \overline{\boldsymbol{\sigma}}(t) + \widetilde{\boldsymbol{M}}_\infty : \boldsymbol{\xi}(t) + \sum_{i=1}^{M-1} \overline{\boldsymbol{M}}_i : \boldsymbol{\beta}_i(t) \quad \text{(E.3)}$$

with

$$\overline{\theta}_i \, \dot{\boldsymbol{\beta}}_i(t) + \boldsymbol{\beta}_i(t) = \overline{\boldsymbol{\sigma}}(t), \ \boldsymbol{\beta}_i(0) = \boldsymbol{0} \quad \text{and} \quad \dot{\boldsymbol{\xi}}(t) = \overline{\boldsymbol{\sigma}}(t), \ \boldsymbol{\xi}(0) = \boldsymbol{0}. \quad \text{(E.4)}$$